Available online at www.sciencedirect.com
SCIENCE DIRECT®
International Journal of Heat and Mass Transfer 49 (2006) 4132–4151
International Journal of HEAT and MASS TRANSFER
www.elsevier.com/locate/ijhmt

Heat transfer at multiple-intermittent impacts of a hollow cone spray ☆

A.L.N. Moreira *, M.R.O. Panão

Instituto Superior Técnico, Mechanical Engineering Department, Av. Rovisco Pais 1049-001 Lisboa, Portugal

Received 3 November 2005
Available online 27 June 2006

Abstract

The present work is aimed at quantifying the effects of frequency in the heat transfer at multiple-intermittent impacts of a hollow cone spray in a way to contribute to the development of advanced heat transfer techniques. The flow configuration is that of a spray impacting perpendicularly onto an aluminium flat plate located at 55 mm. The experiments are conducted at prescribed temperatures ranging from local nucleate/boiling to local transition regimes of heat transfer and with frequencies of injection from 10 Hz to 30 Hz with durations of 5 ms. Analysis is based on spatial resolved measurements of the instantaneous surface temperature during the period of injection, processed in order to obtain estimates of the instantaneous heat flux.

The results show that the local heat transfer is enhanced when the frequency of injection increases from 10 Hz to 20 Hz, but deteriorates with a further increase of frequency, as a clear indication of the interaction between successive intermittent injections. However, the total heat flux removed over the entire area of impact follows the behaviour of typical boiling curves with an *Overall Nukiyama Temperature*. In the overall nucleate boiling regime, the total heat transfer is dominated by a thin film boiling mechanism which lead to breakdown of the liquid at a nearly constant surface temperature, regardless of frequency or any other spray conditions. While at low frequencies this regime is not limited neither by the delivery of liquid to the surface, nor by the removal of vapour from the surface, at higher frequencies it is triggered by enhanced vaporization induced by piercing and mixing the liquid film. A correlation is found for the total heat flux removed from the surface within the nucleate regime which accounts for the combined non-linear effects of surface temperature and pulse frequency,

$$\frac{\langle \dot{\overline{q''}} \rangle}{\dot{m}_f (h_{fg})_b \cdot A_{impact}^{-1}} = 0.17 \cdot \frac{T_w}{T_f} \cdot (\Delta t_{inj} \cdot f_{inj}) - 0.284(\Delta t_{inj} \cdot f_{inj}) + 0.046 \cdot \frac{T_w}{T_f}\left(1 - 0.112\frac{T_w}{T_f}\right) - 0.077.$$

The critical heat flux is shown to be well predicted by correlations reported in the literature for continuous water and dielectric sprays. However, the present multiple-intermittent spray allows achieve higher specific heat fluxes with higher efficiencies.

Keywords: Spray cooling; Pulsed spray; Heat transfer; Overall boiling curve

1. Introduction

Cooling at high heat fluxes is currently a barrier to developing a number of high density power and electronic systems such as those used in space vehicles and satellites, or thermo-photovoltaic systems. Vaporization of a liquid is the only way to achieve such large amounts of heat at low temperatures from small areas and has been considered in most cooling technologies, e.g., Mudawar [1]. In this context, spray cooling allows removing much higher heat fluxes than saturated pool boiling, despite the residence time of the liquid on the surface may be smaller than in a pool. Each individual droplet splash, rebound, spread or stick [2],

☆ Paper submitted to the *International Journal of Heat and Mass Transfer*, revised in March 2005.

* Corresponding author. Tel.: +351 21 841 7875; fax: +351 21 849 6156.
E-mail address: moreira@dem.ist.utl.pt (A.L.N. Moreira).

0017-9310/$ - see front matter © 2006 Elsevier Ltd. All rights reserved.
doi:10.1016/j.ijheatmasstransfer.2006.04.004

Nomenclature

A_{impact}	spray impact area (m^2)
C_p	specific heat (J/kg K)
D	droplet size (μm)
D_{10}	arithmetic mean diameter (μm)
DC	duty cycle ($=[\Delta t_{inj} \cdot f_{inj}] \times 100\%$)
D_{impact}	spray impact diameter (mm)
f_{inj}	injection frequency (Hz)
h_{fg}	latent heat of evaporation (J/kg)
Ja	Jakob number ($C_{p_f} \Delta T_b / h_{fg}$)
k	thermal conductivity (W/m °C)
L_w	plate thickness (mm)
$\dot{m}$	mass flow rate (kg/s)
m_{ev}	total fuel evaporated mass (kg)
m_{inj}	total injected mass (kg)
$\dot{q}''$	instantaneous heat flux (W/m^2)
$\overline{\dot{q}''}$	time-average heat flux (W/m^2)
$\langle \overline{\dot{q}''} \rangle$	total time-average heat flux (W/m^2)
r	measurement radial point (mm)
R_t	overall thermal resistance (W/m^2 °C)
Re	Reynolds number ($=\rho_f DU/\mu_f$)
T	temperature (°C)
t	time instant (s)
T_{amb}	ambient temperature (°C)
T_{inj}	injection cycle time (ms)
T_{ref}	reference temperature (°C)
T_*	limit superheat temperature (°C)
$\langle T \rangle$	overall temperature (°C)
$\langle T_w \rangle_1$	ensemble-average surface temperature of a series of injections (°C)
$\langle T_w \rangle_2$	phase-average surface temperature (°C)
U_r	droplet radial velocity (m/s)
U_z	droplet axial velocity (m/s)
We	Weber number ($=\rho_f DU^2/\sigma_f$)
$\dot{X}_{ev}$	rate of evaporation
z	axial coordinate (mm)

Greek symbols

α	thermal diffusivity (m^2/s)
ΔT_{wb}	degree of superheating ($T_w - T_b$, °C)
Δt	time interval (ms)
ε_{sc}	spray cooling efficiency (%)
ϕ	angular coordinate (°)
φ	dimensionless surface temperature
λ	evaporation constant (m^2/s)
θ	temperature difference ($T_w - T_{bot}$, °C)
μ	dynamic viscosity (kg/m s)
ρ	specific mass (kg/m^3)
σ	surface tension (N/m)
τ	Fourier number
ξ	dimensionless axial coordinate
ξ_{CHF}	coefficient

Subscripts

1D	one-dimensional
304SS	stainless steel alloy
b	boiling or saturation
bot	bottom surface
CHF	at critical heat flux
cr	critical
DP	dead period
f	fuel
inj	injection
N	Nukiyama
p	small perturbations
tc	thermocouple
w	wall

depending on the relative magnitude of the several forces acting upon it (e.g., surface tension, viscous and inertia) and, while spread and stick contribute to form a liquid film on the surface, rebounded and splashed droplets are in contact with the surface only for very short periods of time. In dense sprays, however, the behaviour of single drop impacts is altered by multiple drop interactions, such as those occurring between droplets in the vicinity of each other [3–5] and between consecutive drop impacts [6]. Moreover, when the mass rate of liquid adhered to the surface overcomes the vaporization rate, a liquid film forms which spreads over the surface; crown development and thus secondary atomization is mainly influenced by local variations of the liquid film induced by drop impact; re-atomized droplets may emerge from liquid jets induced by pressure fluctuations generated by multiple drop impacts in the liquid film; interfacial activity in the vicinity of the wall caused by successive injections induce vertical oscillations, which may trigger a chain of ejection-and-re-impaction of droplets with a rate faster than the injection frequency [7,8].

Despite the complexity induced by the interaction between various simultaneous phenomena, heat extraction by spray impingement still follows regimes depending on the temperature of the surface, as in the classical boiling theory. Cooling curves can also be defined which have a maximum value of the heat flux (CHF) occurring at the Nukyiama temperature and a minimum at the Leidenfrost temperature. However, the critical values depend on the dynamics of the spray at impact, e.g., droplet size, number density and momentum, as well as on surface characteristics, such as roughness and wettability. The advantages of spray cooling derive from the cross interaction between

fluid-dynamic and thermal phenomena, as described by Horacek et al. [9]: prematurely break-up of vapour bubbles caused by droplet impingement allow surface rewetting at a higher rate; the entrainment of vapour and air bubbles by droplets to the surface increases the rate of nucleation density and cause vigorous film boiling; the momentum of droplets allows the liquid to get much closer to the surface beyond the Leidenfrost temperature. Furthermore, spray cooling systems allow achieve spatial uniformity and attain higher heat fluxes with lower flow rates, e.g., Estes and Mudawar [10]. Maximum heat fluxes of the order 10^2 W/cm^2 are frequently encountered for continuous water sprays (e.g., Jia and Qiu [11] and Cotler et al. [12]), values up to 1200 W/cm^2 have been reported by Pais et al. [13] for air assisted sprays onto smooth surfaces but further improvements are still required to achieve *ultra high* values of 10^3–10^5 W/cm^2.

It is worth questioning at this point whether intermittent sprays with short pulse duration allows the vapour to be removed more efficiently from the surface, depending on the frequency and duration of injection, and therefore, attaining higher heat dissipation rates with larger efficiencies, as suggested in [14]. Single cryogen spurts with durations of the order of 10–100 ms are currently used to cool the skin before laser treatments of cutaneous vascular lesions, e.g., Aguillar et al. [15] and Kao et al. [16], to permit the safe application of laser pulses with high energy. Multiple cryogen spurts allow better control of the surface temperature and avoid excessive sub-cooling, e.g., [17], and were recently found by Ramirez-San-Juan et al. [18] and Marajon et al. [19] to produce higher cooling rates than continuous sprays. However, none of these studies consider the effects of spray heterogeneities at impact. Dissimilar technological applications include the fuel injection systems of internal combustion engines, where fuel–air mixing depends on the heat transferred at the impact of the fuel spray onto interposed surfaces, e.g., Alkidas [20], Shayler et al. [21,22]. Recent research regarding the effects of multiple droplet interactions induced by successive injections for acceleration enrichment, e.g., [23,24], showed that the cooling curves vary within the area of impact and are shifted by variations of the frequency and duration of injection; the local critical heat flux is reported to be independent of the duration of injection and to vary linearly with the frequency, e.g., [24]. Although the authors were concerned with the resulting effects on fuel–air mixing, the analysis further indicate that injection conditions can be properly used to devise a fast response system to control surface temperature. The present work is aimed at providing further insight into the effects of frequency, which can be used in the development of advanced heat transfer techniques. The experiments consider the lower limit of the dynamic range of a cooling system, for which the liquid is intermittently sprayed with duty cycles $DC = (\Delta t_{inj} \cdot f_{inj}) \times 100\%$ smaller than 20% (where Δt_{inj} is the time of injection and f_{inj} the frequency of successive injections).

In addition, the type of atomization is an important feature of the spray in a surface cooling application. Lateral variations of droplet size, density and velocity induce variations of the thermal interactions within the area of impact and, thus alter the performance of the cooling device. For example, Verkruysse et al. [25] report large differences between two full cone sprays, one with a very small cone angle producing large and high velocity droplets and a spray with a larger cone-angle producing a lesser fine atomization. The authors observed that the heat transfer is enhanced by the piercing of high momentum droplets through the liquid film build up by the jet-like spray, in comparison with the fine atomization spray, which keeps the impacted area dry and forms a liquid film only outside. An experimental study on the flow regimes resulting from the impact of an intermittent hollow cone spray [2] showed that droplets within the high density region interact with the liquid film which forms at early stages of injection at the centerline and spreads outwards at later stages. Here, an additional objective of the analysis is to explore the potential advantages of this pattern for spray cooling applications.

The work derives from a research program devised to study the spray cooling paths which occur in the port fuel injection system of IC engines. Former experiments include simultaneous time resolved measurements of surface temperature and droplet characteristics (e.g., size, velocity and number flux) in a simplified geometry [24], which were processed to provide local phase-average forms of the cooling curves at each location within the area of impact. The maximum and minimum heat fluxes were then associated with *dynamic* Nukiyama and Leidenfrost temperatures, due to their dependency on the injection conditions (e.g., frequency and duration), which induces variations in the heat transfer regimes over the circular impact area. The experiments reported here still consider the use of gasoline, although the approach may generally be applied to other intermittent spray-cooling systems.

2. Experimental method

2.1. Experimental apparatus

The experimental method is described in two previous papers [23,24] together with detailed assessments of measurement accuracy and only a summary is provided here. The flow configuration is depicted in Fig. 1. It consists of an injector spraying gasoline perpendicularly onto a flat aluminium plate located at 55 mm, with thermal diffusivity (α_w) of 6.676×10^{-6} m^2/s and thermal conductivity (k_w) of 164 W/m K. The injector is a BOSCH pintle-type with 0.79 mm of pintle diameter inserted in a hole with 0.9 mm. The fuel spray has a hollow-cone structure with interior and exterior angles of 8° and 19°, respectively, measured with a laser-sheet flow visualization technique.

The injection frequency, pulse duration and number of injections are software controlled by a NI5411 arbitrary

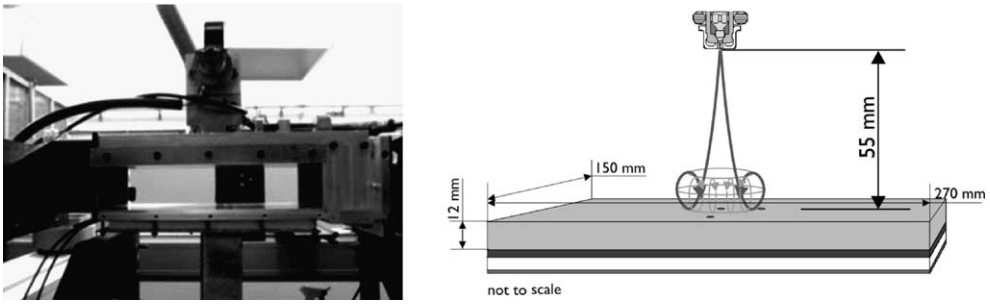

Fig. 1. Flow configuration.

Table 1
Liquid thermophysical properties

Property	Value
Specific mass (ρ_f)	758 kg/m^3
Dynamic viscosity (μ_f)	4.66×10^{-4} kg/m s
Surface tension (σ_f)	19.4 mN/m
Thermal conductivity (k_f)	0.15 W/m K
Boiling temperature (T_b)	60 °C
Critical temperature (T_{cr})	275 °C
Latent heat of evaporation (h_{fg})	346 kJ/kg

function generator from National Instruments (Texas, USA). The fuel used is commercial gasoline and its thermophysical properties are listed in Table 1. The variation of these properties with temperature follows Lefebvre [25].

2.2. Measurement techniques and accuracy

Pressure fluctuations inside the fuel line associated with opening and closing of the injector, generate periodic velocity fluctuations during the period of injection which influence the thermal interaction at impact. The transient behaviour of spray atomization is characterized based on the temporal variations of the droplet velocity and size downstream the exit of the injector. Measurements are made with a two-component phase Doppler DANTEC Dynamics (Denmark) system (PDA) consisting of a 55X transmitting optics, a 57×10 PDA receiving optics and a 58N10 covariance processing unit. Droplet size and velocity are simultaneously measured within the period of injection at a normal distance of 5 mm below the injector nozzle; the axial (U_z) and radial (U_r) velocity directions are aligned and perpendicular to the injector central axis, respectively. Details about the PDA optical configuration are described in Table 2.

The uncertainty in the ensemble-average drop size depends on the deviation from the cumulative size distribution, which can be estimated according to the analysis of Tate [26] as: % Deviation $= 127.32\ \mathrm{N}^{-0.492}$. A maximum deviation of 5% is considered in the cumulative size distribution.

The spatial distribution of the instantaneous temperature at the impacted surface is measured during the period of injection with three NANMAC© fast-response eroding-

Table 2
Optical configuration of the phase Doppler anemometer

Transmitting optics	Value
Laser power	300 mW
Wavelengths	514.5 and 488 nm
Beam spacing	60 mm
Transmitter focal length	500 mm
Frequency shift	40 MHz
Receiving optics	**Value**
Scattering angle	30°
Receiver focal length	500 mm
Processor parameters	**Value**
U and V signal bandwidth	12 MHz
S/N validation	0 dB
Spherical validation	10%

K-type thermocouples, as schematically shown in Fig. 2. In order to ensure that the thermocouples have a low thermal inertia, enabling a response time of the order of 10 μs, the electric resistance was monitored during the experiments and kept between 8 and 12 Ω. Thermocouples are sampled at 50 kHz and the electrical signal amplified with a gain of 300 before processing. Inaccuracies in temperature due to electronic noise increase as the surface temperature decreases and were found to be smaller than ±1% at ambient temperature.

The instantaneous heat flux is calculated from the temperatures measured by the fast response thermocouples at the surface. Analysis shows that lateral conduction is negligible (see Appendix A) and, therefore, the one-dimensional heat conduction may apply with a good accuracy:

$$\frac{\partial \theta}{\partial t} = \alpha \cdot \frac{\partial^2 \theta}{\partial z^2}, \quad \theta(r,z,t) = [T_w(r,z,t) - T_w(r,z,0)] \tag{1}$$

here T_w is the wall temperature, r and z are the radial and axial coordinates, parallel and perpendicular to the wall, respectively. Eq. (1) is solved with the following boundary and initial conditions:

$$\dot{q}''(r,0,t) = -k_w \frac{\partial \theta(r,0,t)}{\partial z} \tag{2}$$

$$\theta(r,L_w,t) = 0 \tag{3}$$

$$\theta(r,z,0) = 0 \tag{4}$$

where L_w is the wall thickness and k_w the thermal conductivity. The boundary condition in Eq. (3) results from the

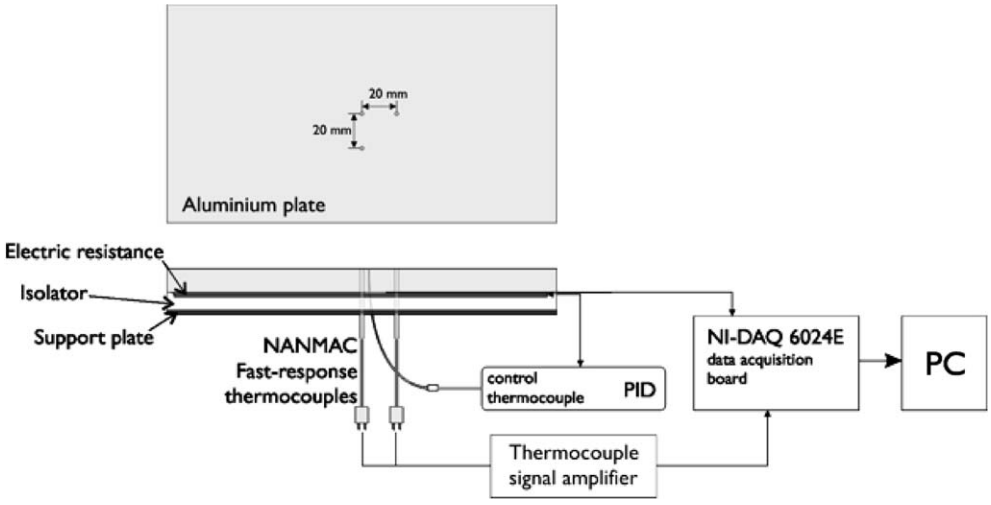

Fig. 2. Schematic of the temperature data acquisition system.

fact that the wall is thick enough so that any temperature fluctuations at the top surface do not propagate to the bottom surface. The differential Eq. (1), is solved after application of a Laplace' transformation as

$$\begin{cases} L\left(\frac{\partial\theta(r,z,t)}{\partial t}\right) = s\theta(r,z,s) - \theta(r,z,0) \\ L\left(\frac{\partial^2\theta(r,z,t)}{\partial z^2}\right) = \frac{\partial^2\theta(r,z,s)}{\partial z^2} \end{cases} \tag{5}$$

giving

$$s\theta(r,z,s) - \theta(r,z,0) = \alpha\frac{\partial^2\theta(r,z,s)}{\partial z^2} \tag{6}$$

The general solution of (6) is

$$\theta(r,z,s) = A\cdot e^{z\sqrt{s/\alpha}} + B\cdot e^{-z\sqrt{s/\alpha}} \tag{7}$$

For the boundary conditions (3) and (4), the solution of (7) is given by

$$\theta(r,z,s) = \frac{\dot{q}''(r,z,s)}{k}\sqrt{\frac{\alpha}{s}}e^{-z/\sqrt{\alpha}} \tag{8}$$

At the top surface ($z=0$) and after some mathematical manipulation using the convolution theorem with $F_1(s) = \frac{\partial\theta(r,0,t)}{\partial t}$ and $F_2(s) = 1/\sqrt{s}$, Eq. (8) becomes

$$\dot{q}''(r,0,t) = \frac{k_w}{\sqrt{\pi\cdot\alpha_w}}\int_0^t \frac{\partial\theta(r,0,t^*)}{\partial t^*}\cdot\frac{1}{\sqrt{t-t^*}}\,dt^* \tag{9}$$

If the time, t, is made dimensionless with the Fourier number, $\tau = \frac{\alpha t}{L_w^2}$ and the integral is calculated as the sum of discrete time intervals between τ_i and $\tau_i + \Delta\tau$, where $\Delta\tau$ is the inverse of the acquisition frequency, Eq. (9) gives:

$$\dot{q}''(r,0,\tau) = \frac{k}{\sqrt{\pi}\cdot L_w}\sum_{k=0}^{i-1}\int_{\tau_k}^{\tau_{k+1}}\frac{dT_w}{d\tau^*}(\tau^*)\cdot\sqrt{\frac{1}{\tau-\tau^*}}\cdot d\tau^* \tag{10}$$

After expanding the derivative in a Taylor series in the interval $[\tau_k, \tau_{k+1}]$ and following the method developed by Reichelt et al. [27], the final result for the instantaneous wall heat flux is given by:

$$\dot{q}''(r,0,\tau_i) = 2\frac{k_w}{L_w}\sqrt{\frac{\Delta\tau}{\pi}}\sum_{k=0}^{i-1}\left[\left(T'_{w,k} + T''_{w,k}\Delta\tau\left(i-\frac{2k+1}{2}\right)\right)\cdot R_{i,k} - T''_{w,k}\frac{\Delta\tau}{3}S_{i,k}\right],$$

$$\begin{cases} T'_{w,k} = \dfrac{T_{w,k+1}-T_{w,k}}{\Delta\tau} \\ T''_{w,k} = \dfrac{(T_{w,k+2}-T_{w,k+1})-(T_{w,k}-T_{w,k-1})}{2(\Delta\tau)^2} \\ R_{i,k} = (i-k)^{1/2} - (i-k-1)^{1/2} \\ S_{i,k} = (i-k)^{3/2} - (i-k-1)^{3/2} \end{cases} \tag{11}$$

Reichelt et al. [27] showed good agreement with the analytical solution for a semi-infinite body with a sinusoidal variation of temperature at the surface, for frequencies greater than 500 Hz. Our experiments are well above this limit and, therefore, inaccuracies are expected to be negligible. Moreover, the time resolution of the method can only be questioned in the low frequency regimes of the order of 0.1 Hz, as pointed out by Chen and Nguang [28].

2.3. Data reduction to process overall boiling curves

Overall boiling curves are built from the time variation of surface temperature measured within the impact area at prescribed surface temperatures at start of injection. In order to ensure a uniform temperature distribution over the impinging surface at the instant of impact, a maximum difference of 1 °C is required between the mean temperatures measured by the three thermocouples, 5 ms before the electronic start-of-injection. Deviations of the uniform

temperature distribution over the plate were found to be less than ±1.12% between the three thermocouples for all the experimental conditions.

After the target plate has been heated up to the desired temperature, consecutive injections are performed and temperatures are continuously sampled at 50 kHz at each location on the surface. The procedure is stopped and re-initialized to re-heat the plate. It was tentatively found that seven consecutive injections ensure that surface temperature at start of each injection drops less than 5% for all experimental conditions and therefore, the heat transfer regime remains unchanged during each experiment. A mean time-series of seven consecutive injections is then obtained from N_{series} measured series.

$$\langle T_{\text{w}}(r,0,t)\rangle_1 = \frac{1}{N_{\text{series}}}\sum_{i=1}^{N_{\text{series}}} T_{\text{w}}^{i\text{th series}}(r,0,t) \tag{12}$$

A validation procedure is devised to ensure the temperature distribution is uniform at start of injection and then the instantaneous temperature during injection, $\langle T_{\text{w}}(r,0,t)\rangle_2$, is obtained by phase averaging:

$$\langle T_{\text{w}}(r,0,t)\rangle_2 = \langle T_{\text{w}}(r,0,0)\rangle_1^{1\text{st}} + \frac{1}{N_{\text{vinj}}}\sum_{i=1}^{N_{\text{vinj}}}(\langle T_{\text{w}}(r,0,t)\rangle_1 - \langle T_{\text{w}}(r,0,0)\rangle_1)^{i\text{th valid injection}} \tag{13}$$

In this procedure, the first injection was always rejected because it finds peculiar boundary conditions. The averaging process allows smooth the variability of transient temperature profiles observed for equal working conditions, as also reported by Labeish [29]. Error analysis showed that inaccuracies induced in the instantaneous heat flux are smaller than 2%.

Around 70 series of seven injections are performed during which temperature variations at the top surface are measured. The instantaneous heat fluxes, $\dot{q}''(r,0,t)$, are then calculated from the phase-averaged temperature, $\langle T_{\text{w}}(r,0,t)\rangle_2$, in a post-process algorithm implemented in Matlab®, according to the algorithm in Eq. (11). Thereafter, the heat flux is integrated to give the time-average heat flux removed from the wall at each measurement location during the period of injection (T_{inj})

$$\overline{\dot{q}''}(r,0) = \frac{1}{T_{\text{inj}}}\int_0^{T_{\text{inj}}} \dot{q}''(r,0,\tau)\,\mathrm{d}\tau \tag{14}$$

The integral is calculated numerically using the composed trapezes rule of integration. Because of the relatively high sample rate, the integration error is negligible. The total average heat flux removed over the entire area of impact is then calculated as:

$$\langle\overline{\dot{q}''}\rangle = \frac{\pi}{A_{\text{impact}}}\int_{-R}^{R}\overline{\dot{q}''}(r,0)\,\mathrm{d}r \tag{15}$$

from which *overall boiling curves* are calculated for each injection condition.

2.4. Dimensional analysis – the route to compare with other experiments

Extrapolation of the results obtained here to spray-cooling applications using other fluids, can be made only by proper scaling the influence of liquid properties on the several phenomena involved in the thermal interaction at impact. Firstly, the thermal outcome depends on the relative magnitude of the several forces acting upon each individual droplet at impact (e.g., surface tension, inertia and viscous) since these determine the fluid-dynamic interactions and, therefore, the contact time available for thermal interaction. These mechanisms of interaction are described by dimensionless numbers expressing the relative magnitude of those forces, usually the Weber ($We = \rho_{\text{f}} D U^2/\sigma_{\text{f}}$) and Reynolds ($Re = \rho_{\text{f}} D U/\mu_{\text{f}}$) numbers. On the other hand, heat is removed from the surface by sensible heating the liquid up to the boiling point and by liquid vaporization. The former is scaled here by the sensible heat required to heat the liquid from the ambient to the boiling temperature, $C_p(T_{\text{b}} - T_{\text{amb}})$, the second is scaled with the evaporation constant, λ, of the d^2 *law* of vaporization, $t = D^2/\lambda$. The ratio of the sensible to the latent heat determines the cooling efficiency and may be scaled by the Jacob number at the boiling point, $Ja = C_p(T_{\text{b}} - T_{\text{f}})/h_{\text{fg}}$. Table 3 compares the above scales with those estimated for other common liquids used in spray-cooling of electronic systems and dermatological applications.

A cooling efficiency may also be defined as the ratio of the total average heat flux removed over the entire area of impact, $\langle\overline{\dot{q}''}\rangle$, to the maximum which would have been removed if all the thermal energy for complete vaporization of the spray have been received from the surface, $\langle\overline{\dot{q}''}\rangle_{\max}$:

$$\langle\overline{\dot{q}''}\rangle_{\max} = \frac{\dot{m}_{\text{f}}\cdot\Delta t_{\text{inj}}\cdot f_{\text{inj}}}{A_{\text{impact}}}[C_{p_{\text{f}}}(T_{\text{b}} - T_{\text{f}}) + h_{\text{fg}}] \tag{16}$$

where $\dot{m}_{\text{f}}$ is the mass flow rate, Δt_{inj} the pulse duration, f_{inj} the injection frequency, A_{impact} the impact area ($0.25\pi D_{\text{impact}}^2$), T_{b} is the liquid boiling temperature, T_{f} the liquid temperature and finally, $C_{p_{\text{f}}}$ and h_{fg} are the liquid specific heat and latent heat of evaporation, evaluated at a reference temperature, respectively, defined as

Table 3
Dimensionless numbers scaling gasoline with common cooling liquids

Fluid (*)	$\frac{We_{\text{GAS}}}{We_*}$	$\frac{Re_{\text{GAS}}}{Re_*}$	$\frac{C_p(T_{\text{b}}-T_{\text{amb}})_{\text{GAS}}}{C_p(T_{\text{b}}-T_{\text{amb}})_*}$	$\frac{Ja_{\text{GAS}}}{Ja_*}$	$\frac{\lambda_{\text{GAS}}}{\lambda_*}$
FC-87[(1)]	0.23	0.508	13.337	2.595	0.637
FC-72[(1)]	0.213	0.529	2.151	0.419	0.779
FC-77[(1)]	0.189	0.499	0.86	0.159	[a]
H_2O[(2)]	3.126	1.983	0.231	1.3691	5.829
R-134[a (2)]	0.297	0.328	0.981	0.469	0.637

Sources: (1) 3 M.
(2) National Institute of Standards and Technology (USA).
[a] Not estimated.

$$T_{\mathrm{ref}}(T)=\begin{cases} T_{\mathrm{b}}-\frac{T-T_{\mathrm{b}}}{3} & \text{if } T>T_{\mathrm{b}} \\ T-\frac{T_{\mathrm{b}}-T}{3} & \text{if } T<T_{\mathrm{b}} \end{cases} \quad (17)$$

The relative magnitude of the sensible to the latent heat in (16) was estimated to be smaller than 16.4% for all experimental conditions.

The efficiency of the spray cooling, $\varepsilon_{\mathrm{sc}}$, is finally calculated by

$$\varepsilon_{\mathrm{sc}}=\frac{\langle\dot{\bar{q}}''\rangle}{\langle\dot{\bar{q}}''\rangle_{\max}}\times 100\% \quad (18)$$

3. Results and discussion

The results are presented and discussed in this section under three headings. The first two consider the effects of injection frequency on the transient behaviour of the spray during the period of injection: the former addresses the dynamics of atomization; the second the heat transferred upon impact. The third sub-section analyzes the overall process of heat transfer, based on an integral methodology which accounts for the heterogeneities of fluid-dynamic interactions induced by multiple-intermittent injections within the area of spray impact. Here, *overall boiling curves* are built from transient heat fluxes obtained for several injection frequencies and the results discussed in term of the spray cooling potential and efficiency.

The experiments were conducted at prescribed temperatures at the start of injection ranging from 125 °C to 225 °C, which cover the local nucleate/boiling ($T_{\mathrm{b}}<T_{\mathrm{w}}<T_{\mathrm{Nukiyama}}$) and the local transition ($T_{\mathrm{Nukiyama}}<T_{\mathrm{w}}<T_{\mathrm{Leidenfrost}}$) regimes of heat transfer, as defined by Naber and Farrel [30] and illustrated in Fig. 3: in the nucleate/boiling regime, bubbles emerge from the surface due to nucleation; in the *transition* regime, the liquid is in contact with the surface only intermittently, due to separations from the surface caused by vapour expelled from the liquid.

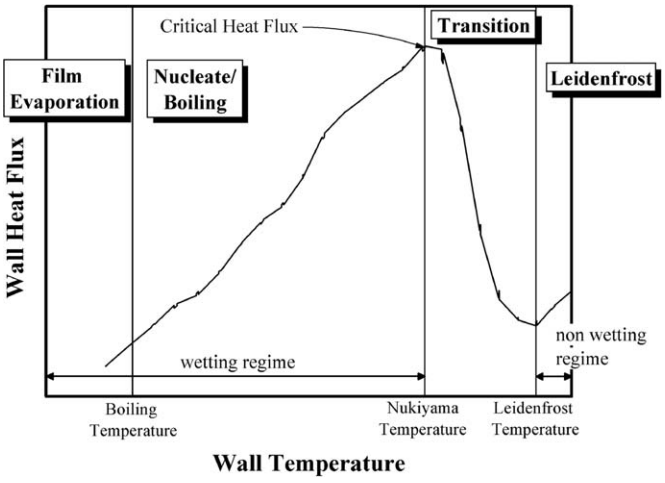

Fig. 3. Typical boiling curve with illustration of the heat transfer regimes.

The frequency of injection varies from 10 Hz to 30 Hz; the duration (Δt_{inj}) is kept constant and equal to 5 ms, with duty cycles DC = $(\Delta t_{\mathrm{inj}}\cdot f_{\mathrm{inj}})\times 100\%$ at 5%, 7.5%, 10% and 15% and the pressure of injection is set to 3 bar. The temperature of the fuel is monitored and kept constant during all experiments at 32 °C.

3.1. Effect of injection frequency on the transient behaviour of the spray atomization

An important feature of multiple-intermittent spray cooling is that the resulting liquid spray is not only pulsed, but it is also transient during the period of injection due to pressure variations inside the liquid line, which occur in a time scale of the same order of magnitude as the duration of injection. This is an important feature which has to be accounted for when describing the thermal-fluid dynamics of the impact. The transient behaviour of the injector may be divided in three periods, as described in [24] and illustrated in Fig. 4 in terms of the mean axial velocity and size of droplets for durations of injection of 5 ms and 10 ms: (i) the first period, or the *leading front of the spray*, is characterized by a sudden expansion of the liquid after pintle opening, resulting in a local minimum of the mean axial velocity at the end of the period and a large negative gradient of the mean drop size; (ii) the second period, *the steady spray*, starts when the mean drop size attains a plateau value; it lasts up to the end of injection and the mean droplet axial velocity increases up to a steady value; (iii) in the third and final period, which corresponds to the *spray tail* and starts after the end of injection, only small droplets remain suspended in the air with a mean axial velocity decreasing asymptotically down to 0 m/s.

A qualitative picture of the transient behaviour of the spray at the three time stages is given in the sequence of photographs shown in Fig. 5, obtained at a frequency of injection of 10 Hz. Complementarily, Figs. 6 and 7 depict the size and velocity distributions, respectively, measured at 5 mm below the injector at radial positions associated with (i) the hollow region of the spray ($r=0$ mm), (ii) the dense part of the spray ($r=1$ and 2.5 mm) and (iii) the edge of the spray ($r=3.5$ mm). The first droplets arrive at the PDA measurement volume 2 ms after the electronic start of injection, which includes the electromechanical delay.

The figures show that: (i) droplets issue from the nozzle with a larger cone angle during the *leading front of the spray*, which lasts up to 1 ms after start of injection and atomization results in a large dispersion of size and velocity of droplets; (ii) the cone angle then decreases and remains constant during the *steady* period, which lasts up to 7 ms after start of injection; although the size distribution is rather dispersed ($r=1$ mm), a significant number of small (≈30 μm) and relatively slower droplets (≈14 m/s) can be detected in the vicinity of the outer boundary of the spray ($r=2.5$ mm); (iii) the cone angle increases again during the *tail* of the spray, which lasts up to disappearance of all

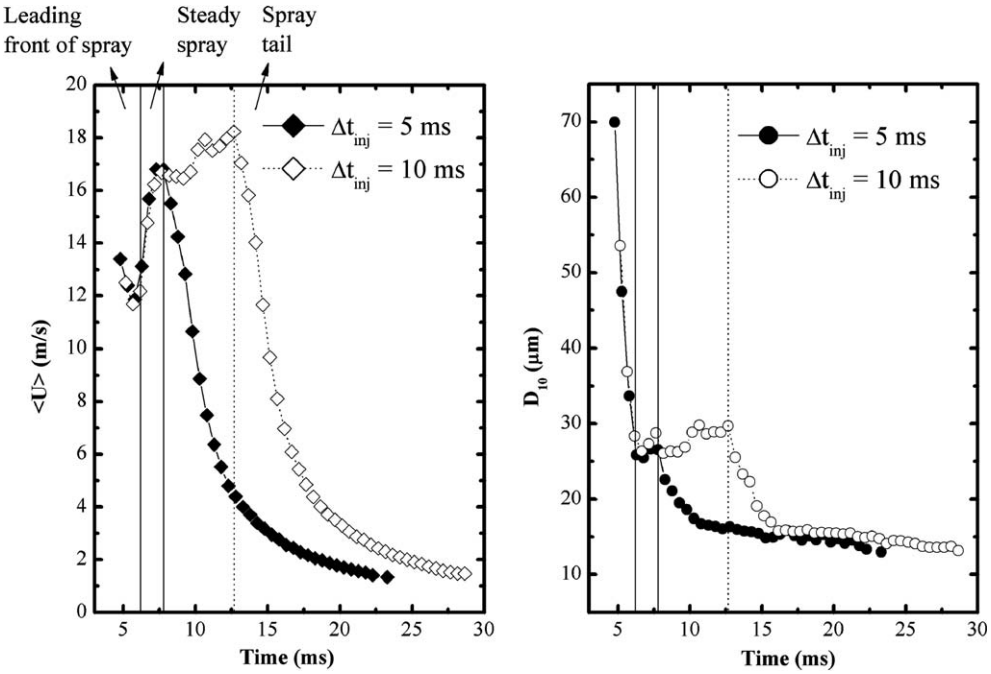

Fig. 4. Transient behaviour of the spray in terms of the mean axial velocity ($\langle U \rangle$) and size (D_{10}) of droplets.

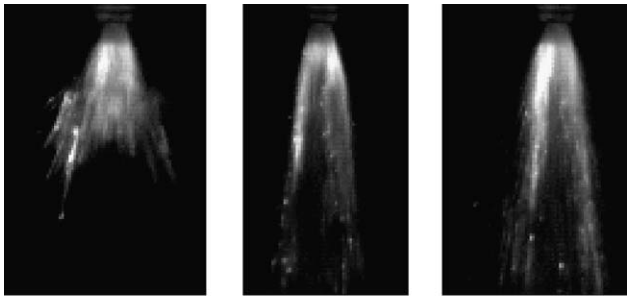

Fig. 5. High speed photographs of the spray injected at 10 Hz obtained along the time of injection at: (a) $t^* = 0.05$; (b) $t^* = 0.25$; (c) $t^* = 0.85$. ($t^* = t_i/\Delta t_{inj}$; $\Delta\ t_{inj} = 10$ ms and $p_{inj} = 3$ bar).

droplets and is characterized by a fast reduction of velocity, due to the rapid loss of the driving momentum and by a wide size distribution, with drop sizes up to 100 μm.

The direct implication of unsteadiness on the impact is that the average droplet size and velocity vary during an injection cycle. Therefore, impinging droplets will interact in a complex way around the impact area and describing this flow as a superposition of single droplets is not fully accurate as shown by Tropea and Roisman [4]. Here, it is particular important to identify the effect of injection frequency on the transient behaviour of the spray.

Fig. 8 shows the effects on the time varying radial distributions of ensemble-average axial velocity measured at 5 mm from the nozzle. Although the transient pattern does not change significantly with frequency, the axial velocity of droplets at the edge of the spray increases with frequency, as depicted by the arrows in the figure.

Fig. 9 complements the analysis and shows the resulting effects on the normalized droplet number density measured at frequencies of 10 and 30 Hz. In general the results quantify the larger angle of the spray during the leading front and show that droplet density is at the outskirts of the spray increase with frequency.

The implication is that, as the frequency increases from 10 Hz to 30 Hz, relatively more and faster drops are expected to strike the wall at the outer edge of the impacted area. The resulting effects on the thermal interaction are quantified in the following paragraphs.

3.2. The effect of injection frequency on the local time variations of surface temperature and heat flux

Figs. 10a and b depict the effect of frequency on the time variation of the measured temperature and of the calculated heat flux, at two typical radial locations, which characterize, respectively, the core region of high droplet density (Fig. 10a) and the outward region, which is wetted by the spray tail and is dominated by the vortical structure induced by intermittent injection (Fig. 10b). The experiments were performed at different surface temperatures below the Leidenfrost regime. However, since the effects are not qualitatively affected by the initial surface temperature, only $T_w = 125$ °C is represented, which corresponds to the local nucleate boiling regime [24].

At the core of the impacted area, the temperature and heat flux curves qualitatively resemble each other and show a thermal morphology similar to that observed at the impact of single droplets, e.g., Labeish [29]. Each curve can be divided in four regions in terms of their slopes. After a steady period before spray impact, measured temperature

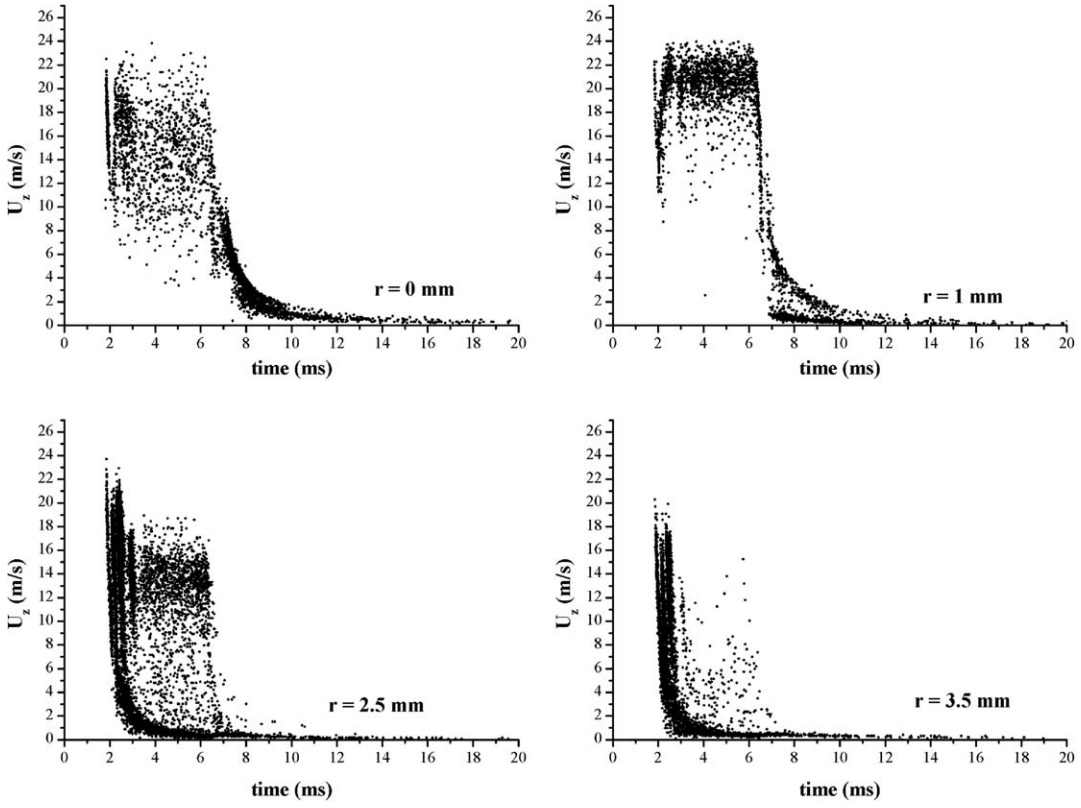

Fig. 6. Scatter plot of droplet axial velocity measured at 5 mm from the exit of the nozzle with $f_{inj} = 10$ Hz.

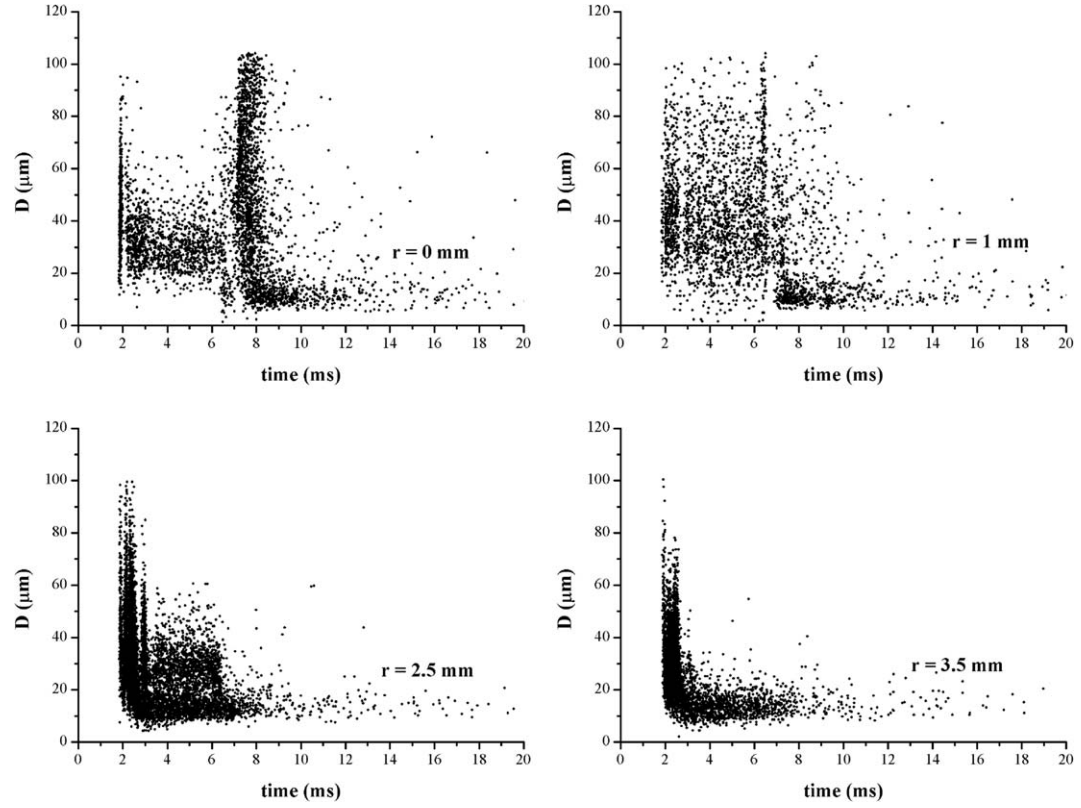

Fig. 7. Scatter plot of droplet size measured at 5 mm from the exit of the nozzle with $f_{inj} = 10$ Hz.

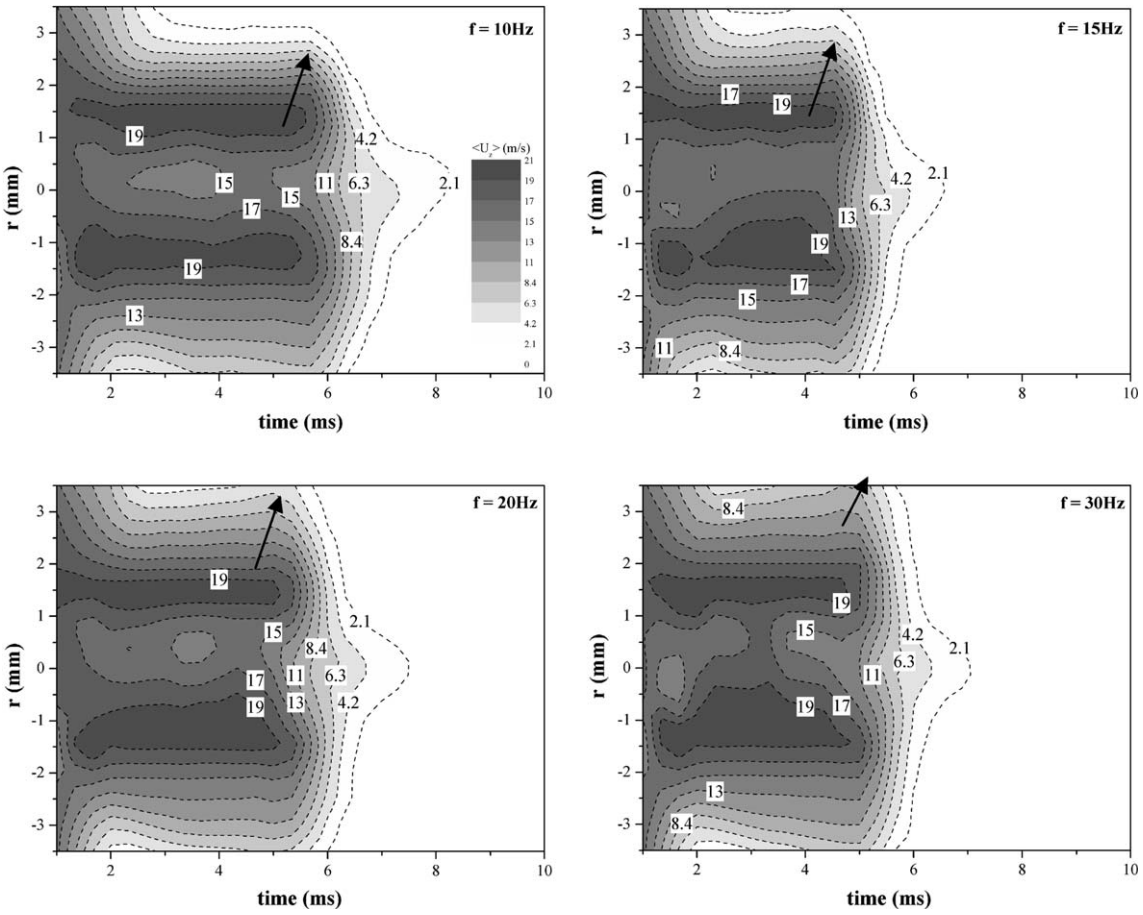

Fig. 8. Radial transverses of the droplet axial velocity during the time of injection and for $f_{inj} = 10$, 15, 20 and 30 Hz.

decreases sharply in Region I due to fast vaporization of leading droplets, as reported by Chen and Hsu [31], and the heat flux reaches an absolute maximum, $\dot{q}''_{max}$; in Region II surface temperature reaches a minimum, $\min(T_w)$, but the rate of temperature decay decreases and the heat flux remains almost constant or even slightly decreases, which may be associated with build up of a liquid film and lower vaporization rates, as also observed by Labeish [29]; in Region III, measured temperatures increase due to complete evaporation of the residual liquid. This description is associated with a thermal morphology which changes from a non-wetting regime right after spray impact to a regime associated with a short contact between the liquid and the target.

The results in Fig. 10a further show that the frequency of injection quantitatively alters the above described trend, as a clear indication of the interaction between successive intermittent injections: the rate of temperature decay, as well as the instantaneous heat flux, increases when the frequency of injection increases from 10 Hz to 20 Hz, but decreases with a further increase of frequency. A similar deterioration of the heat flux as that reported here for a duty cycle DC = 0.15 has also been reported for a cryogenic spray imparting onto a cooper surface by Majaron et al. [19], but for duty cycles above 0.70. It is rather speculative to attribute the differences to a faster rate of vaporization of cryogenic droplets, since this is known to be strongly dependent on spray dynamics, e.g., droplet size, velocity and number density, as also reported by Aguillar et al. [32]. The argument here is that the phenomena is not scaled by the duty cycle. Instead, interaction between successive spurts is expected to occur if the mass of liquid remaining after spurt termination is more than the system is able to vaporize before the next spurt. If the total mass of liquid injected onto the surface, m_{inj}, is given by

$$m_{inj} = \dot{m} \cdot \Delta t_{inj} \tag{19}$$

where $\dot{m}$ is the mass flow rate of liquid issued by the nozzle; the total mass vaporized during the period of injection, $(m_{ev})_{inj}$, is given by

$$(m_{ev})_{inj} = (\dot{X}_{ev})_{inj} \cdot \Delta t_{inj} \tag{20}$$

where $(\dot{X}_{ev})_{inj}$ is the rate of evaporation; and the mass of liquid vaporized in the time between spurts, t_{DP}, given by

$$(m_{ev})_{DP} = (\dot{X}_{ev})_{DP} \cdot \Delta t_{DP} \tag{21}$$

where $(\dot{X}_{ev})_{DP}$ is the rate of vaporization within the corresponding period, then interaction occurs if $[m_{inj} - (m_{ev})_{inj}] > (m_{ev})_{DP}$. Rearranging and assuming that the rate of film vaporization is equal to the vaporization rate during

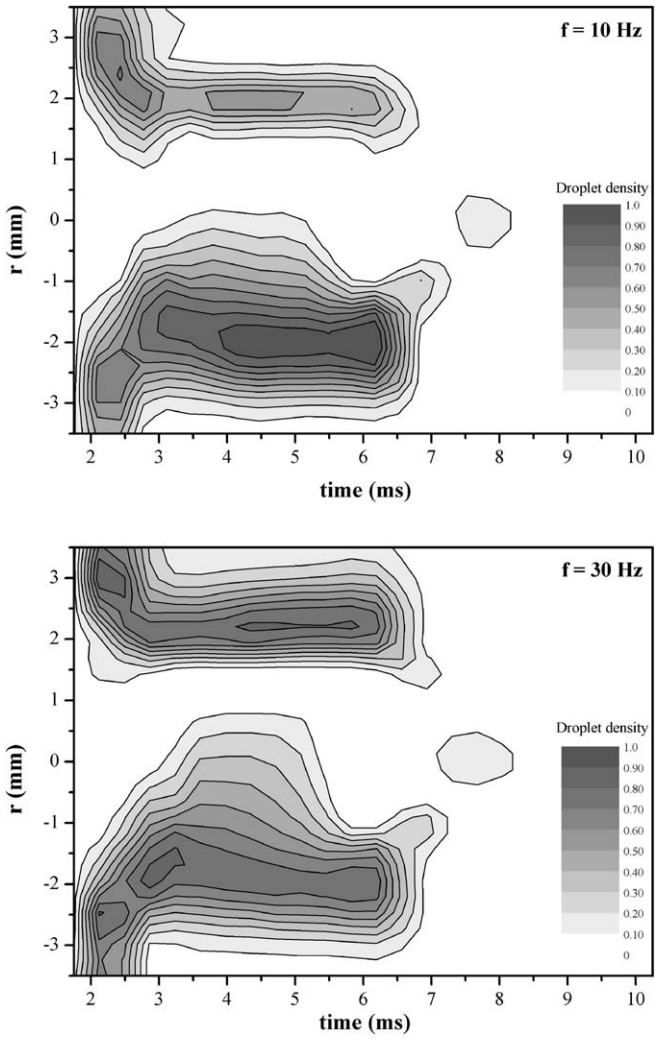

Fig. 9. Radial transverses of the droplet density during the time of injection and for $f_{inj} = 10$, 15, 20 and 30 Hz.

injection, $(\dot{X}_{ev})_{inj} = (\dot{X}_{ev})_{DP} = \dot{X}_{ev}$, the condition can be expressed in terms of the duty cycle, DC, as:

$$\left(\frac{\dot{m}}{\dot{X}_{ev}} - 1\right) \cdot \frac{DC}{1 - DC} > 1 \tag{22}$$

Furthermore, according to the D^2 law for evaporation, the rate of vaporization of gasoline droplets is of the same order of magnitude of that of cryogen droplets of the same size. Therefore, the condition for interaction between successive injections is fulfilled in the present work with smaller duty cycles solely because the mass flux is larger. This question is relevant if the present results are to be compared with other experiments reported in the literature.

The transient thermal behaviour at the outward region is much more complex (see Fig. 10b): absolute values of the heat flux are in average four times smaller than within the central region and a second peak is observed in the time variation of the heat flux associated with re-impingement of the secondary droplets entrained by the wall vortex; temperature curves in Region II move from low- to a high-gradient pattern as the frequency of injection increases, which is attributed to the increased ability of successive spurts to de-wet the outer region of impact.

An overview of the above described trends is shown in Fig. 11, which represents the most important parameters of the cooling curves, which are relevant to evaluate the performance of a cooling technology. These are the dimensionless minima surface temperature $\min(\varphi)$, where $\varphi(t) = (T_w(t) - T_f)/(T_w(0) - T_f)$, and the time $t_{\min(\varphi)}$ at which $\min(\varphi)$ occurs, the maxima heat flux, $\dot{q}''_{max}$, and the time $t_{\max(qw)}$ at which $\dot{q}''_{max}$ occurs. All quantities are shown within the area of impact for several values of the surface temperature at start of injection. In general, the results show that, within the core region, $\min(\varphi)$ is always reached before spurt termination as also reported by Ramirez-San-Juan et al. [18], because liquid superheating $(T_w - T_b)$ and mass flow rate are much larger in the present work. However, the time to reach $\min(\varphi)$ increases significantly at the outwards region, due to the fluid-dynamic nature as it moves away from the centre of the flow, there: droplet number density is smaller; and the liquid film becomes thicker, taking more time to reach the saturation temperature. It is likely that single-phase heat transfer is dominant at the outwards area of impact. Note, however, that the behaviour of all parameters is insensitive to the frequency of injection and, also, the magnitude of either, $t_{\min(\varphi)}$ and $t_{\max(qw)}$ show a negligible dependence on the initial temperature of the target. The main effect of frequency is seen on the absolute values of instantaneous temperature and heat flux, particularly in the vicinity of the centreline, where the corresponding peak values decrease when the frequency increases from 20 Hz to 30 Hz.

Integration of the instantaneous heat fluxes within the period of liquid injection allows comparing the net effects of the frequency on the cooling performance. Figs. 12a–c present the surface density of thermal energy removed along a radial transverse during each injection for surface temperatures from 125 °C to 175 °C. In general, the results confirm the heterogeneous structure of spray impact, though showing a symmetric behaviour, and the deterioration of the heat transfer rate at 30 Hz in the vicinity of the centreline. However, it is worth noting that the total amount of heat removed by the spray per unit time increases with frequency, because more mass of liquid is supplied to the surface, [33]. Interaction of impacting droplets with the dynamic liquid film which occurs at increased frequencies is the main mechanism preventing fast de-wetting between successive spurts but, for the experimental conditions reported here, it only sets a limitation to the cooling efficiency.

The analysis to this point provides explanations of the physical nature of the transient heat removal with multiple-intermittent sprays. From the point of view of the system performance it is also important to consider the total cooling rate in a way that accounts for the complex interactions induced by spatial heterogeneities. This is addressed in the following section.

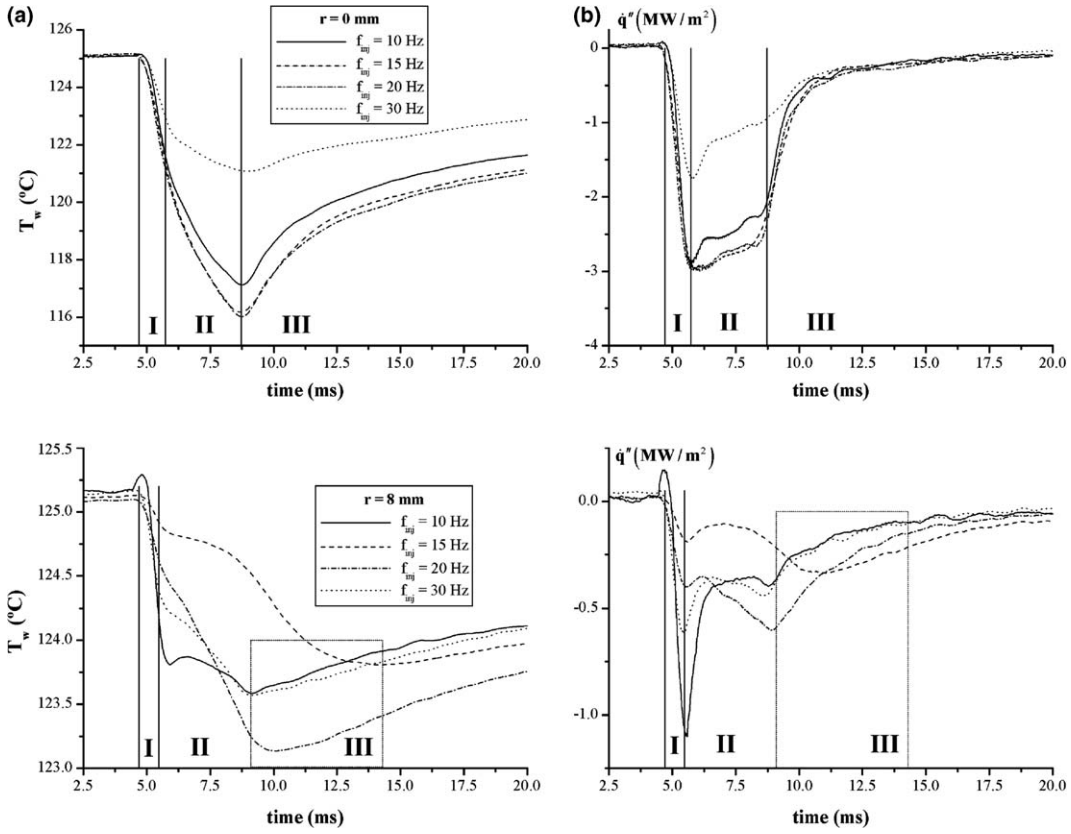

Fig. 10. Effect of the injection frequency on the transient profiles of the surface temperature for 150 °C at $r = 0$, 2, 4 and 6 mm (a) and corresponding heat flux (b).

3.3. Effect of the injection frequency on the overall cooling efficiency

The time average heat flux has been integrated within the area of impact ($D_{\text{impact}} = 40$ mm) as given by Eq. (13) and the results are shown in Fig. 13 as a function of the superheating degree, $\Delta T_{\text{wb}} (= T_{\text{w}} - T_{\text{b}})$. The curves show a behaviour similar to typical boiling curves with a critical temperature at which the total amount of heat removed from the surface for each frequency of injection is maximum. Surprising is the fact that, despite the frequency of injection alters the transient behaviour of the cooling curves, it has a negligible influence on the critical temperature, which is shown to be around $(\Delta T_{\text{wb}})_{\text{CHF}} = 140$ °C for all the experimental conditions reported here. The overall effect of frequency is seen in the cooling efficiency defined by Eq. (18) and represented in Fig. 14 as a function of the dimensionless temperature expressed by the Jacob number. The results show a monotonic decrease of the overall efficiency with increasing frequency only below the critical surface temperature. The analysis then supports the evidence that the critical temperature sets a transition between *overall* heat transfer regimes (see Fig. 3): the impact area is dominated by local nucleate boiling at lower temperatures and by local intermittent transition regimes at higher temperatures. Therefore, the curves in Fig. 13 are henceforth named *Overall Boiling Curves* and the critical temperature *Overall Nukiyama Temperature*.

If the efficiency is estimated such as all the heat would have been removed by single-phase mechanism:

$$\varepsilon^* = \frac{C_{p_{\text{f}}} \cdot (T_{\text{w}} - T_{\text{b}})}{[C_{p_{\text{f}}} \cdot (T_{\text{w}} - T_{\text{b}}) + h_{\text{fg}}]} \times 100\% \tag{23}$$

then it would give values ranging from $\varepsilon^* = 14.5\%$ at $T_{\text{w}} = 125$ °C up to $\varepsilon^* = 30\%$ at $T_{\text{w}} = 225$ °C. Fig. 14 shows that, regardless frequency, maxima efficiencies occur at the *Overall Nukiyama Temperature*, $\langle T \rangle_{\text{N}}$. But, while the maximum efficiency for 10 Hz and 15 Hz is approached with an increment of the order of the corresponding increment due to sensible heat, it is evident for frequencies of 20 Hz and 30 Hz that the critical heat flux is associated with a sudden increase of the rate of phase change. Although it is not possible to provide the exact nature of this behaviour, boiling of a thin film at Critical Heat Flux was shown by Kopchikov et al. [34] to be a thermodynamic critical phenomena which occurs at a temperature difference $[(\Delta T_{\text{wb}})_{\text{CHF}} = \langle T \rangle_{\text{N}} - T_{\text{b}}]$ correlated with the limit temperature difference $(\Delta T_* = T_* - T_{\text{b}})$. Here T_* is the limit superheat temperature at which the liquid is in a thermodynamic stable state evaluated as $T_* = (27/32) T_{\text{cr}}$. This correlation is linear and proportional to ξ_{CHF} as $(\Delta T_{\text{wb}})_{\text{CHF}} = \xi_{\text{CHF}} \Delta T_*$. In our experiments, $\xi_{\text{CHF}} = 0.814$ for $(\Delta T_{\text{wb}})_{\text{CHF}} = 140$ °C, which

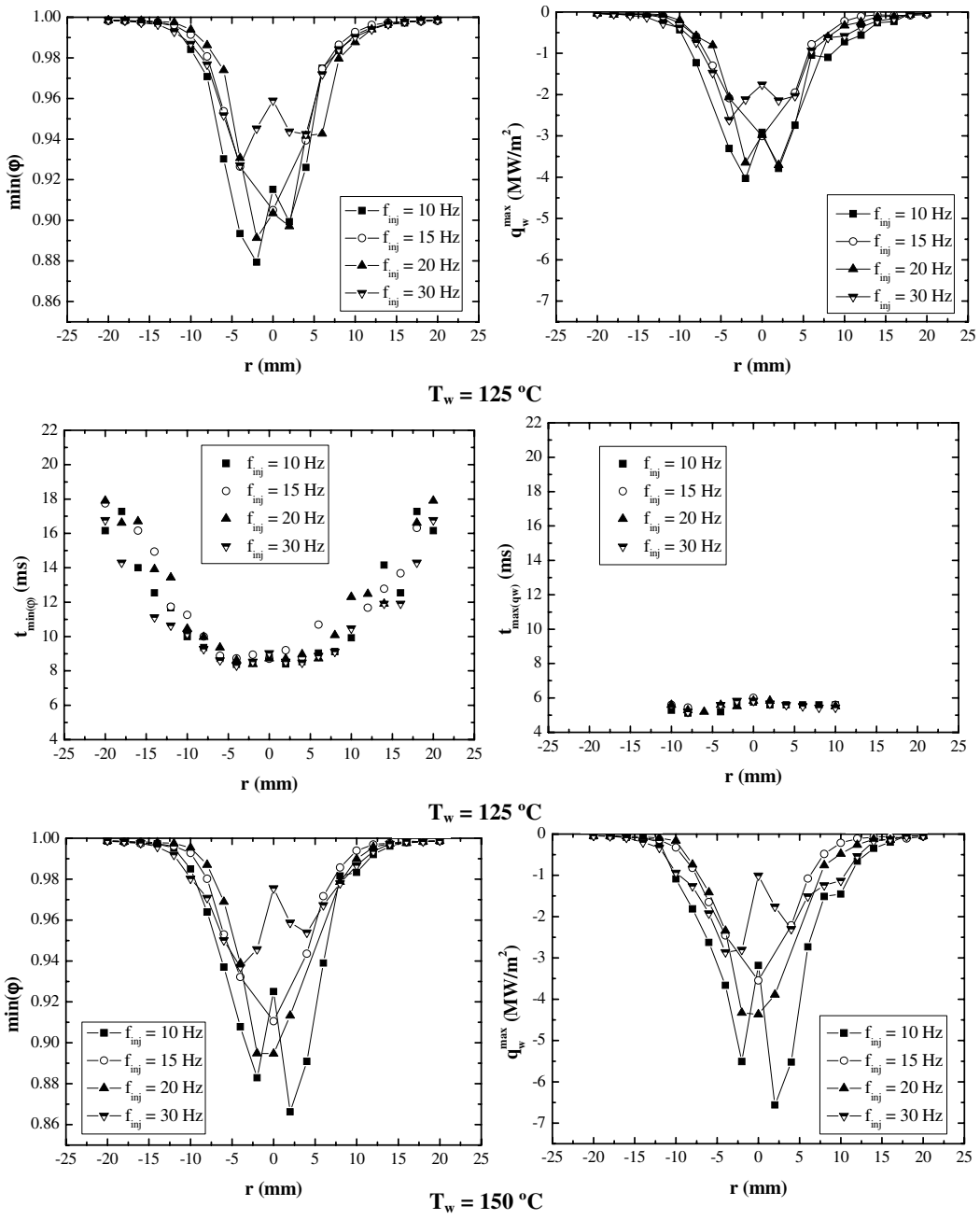

Fig. 11. Radial traverses of: minimum surface temperature $T_{\min}$, and the time $\tau_{T\min}$ at which $T_{\min}$ occurs; maximum heat flux, $\dot{q}''_{\min}$, and the time $\tau''_{\dot{q}_{\max}}$ at which $\dot{q}''_{\min}$ occurs, for (a) $T_w = 125$ °C; (b) $T_w = 150$ °C; (c) $T_w = 175$ °C.

is close to the value 0.83 obtained by Kopchikov et al. [34]. This means that the *Overall Critical Heat Flux* is dominated by a thin film boiling mechanism, which leads to breakdown of the liquid at a nearly constant surface temperature, regardless of frequency or any other spray conditions. While at low frequencies this mechanism is not limited neither by the delivery of liquid to the surface, nor by the removal of vapour from the surface as in Pautsch and Shedd [35], at higher frequencies, piercing of impinging droplets and mixing of the liquid film occurs sooner during the period of temperature recovery, as in Rini et al. [36] and Shedd and Pautsch [37]. The result is an increase of the heat extracted from the wall although with less efficiency.

A major concern here is to attempt to devise a mechanism to control the temperature of the surface when the system is dynamic. Fig. 15 shows the overall cooling efficiency versus the overall heat flux for fixed values of the surface temperature, obtained for all conditions tested, with indication of the frequency of injection. The results show that, to operate the surface at a particular constant temperature below the *overall Nukiyama temperature* ($T_w \leqslant 175$ °C), the frequency of injection has to be increased as the heat released by the device increases. But, for temperatures

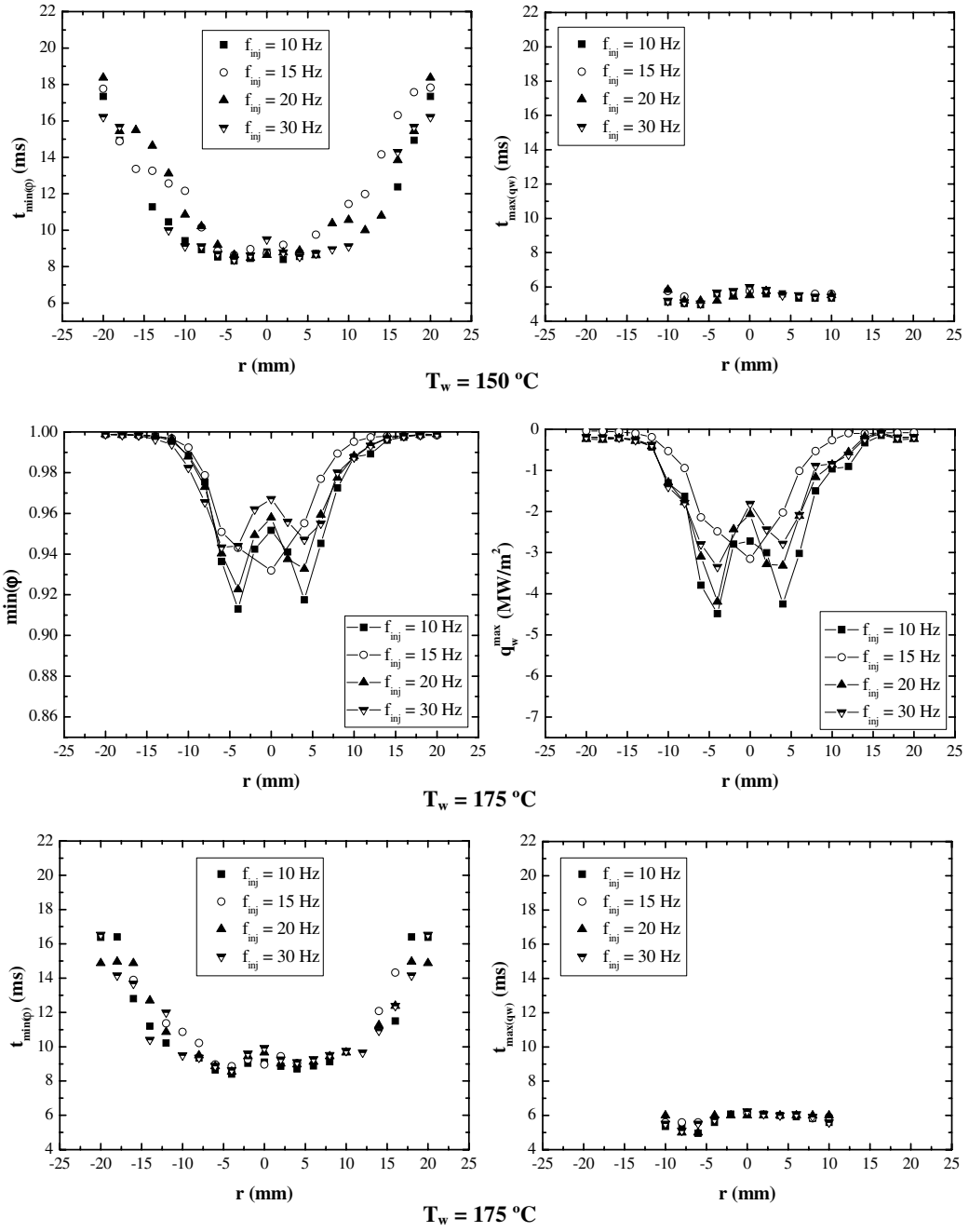

Fig. 11 (*continued*)

above 200 °C it is not possible to devise any trend useful for a control system (see Fig. 16). The reason is associated with the fact that the total average heat flux $\langle \overline{\dot{q}''} \rangle$ varies linear with the frequency at the *overall nucleate boiling* region (see Fig. 16), expressed in normalized terms as:

$$\frac{\langle \overline{\dot{q}''} \rangle}{\dot{m}_f (h_{fg})_b \cdot A_{impact}^{-1}} = a_f \cdot (\Delta t_{inj} \cdot f_{inj}) + b_f \tag{24}$$

where $\dot{m}_f$ is the injector mass flux at 3 bar and $(h_{fg})_b$ is the latent heat of evaporation and A_{impact} is the total spray impact area. The rate of variation of a_f and b_f depends on the surface temperature normalized by the fluid temperature, i.e.:

$$\begin{aligned} a_f &= a_f^{(1)} \cdot \frac{T_w}{T_f} + a_f^{(0)} \\ b_f &= b_f^{(2)} \cdot \left(\frac{T_w}{T_f}\right)^2 + b_f^{(1)} \cdot \frac{T_w}{T_f} + b_f^{(0)} \end{aligned} \tag{25}$$

The experiments allow to estimate the coefficients in Eq. (25) as shown in Table 4 and to find a correlation for the normalized *overall average heat flux* within the nucleate regime:

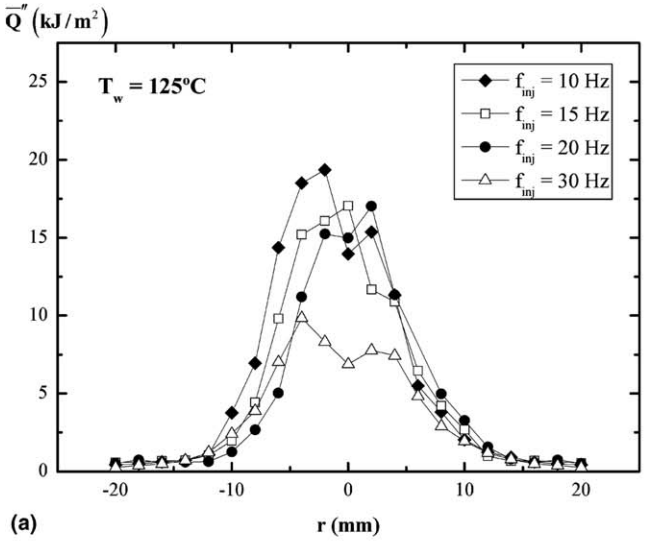

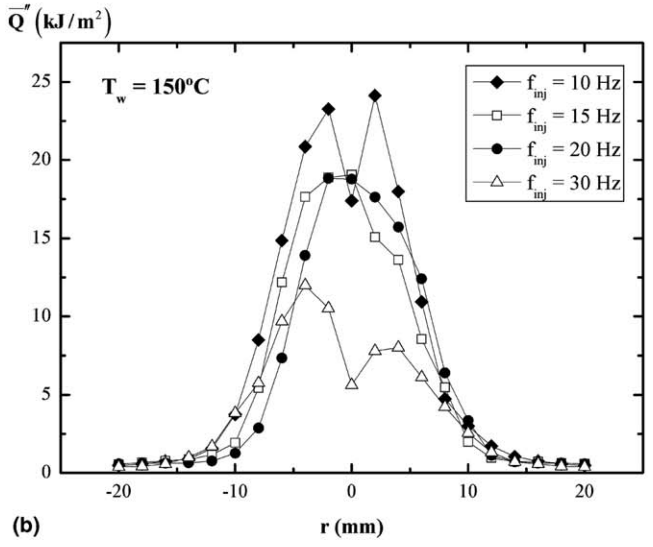

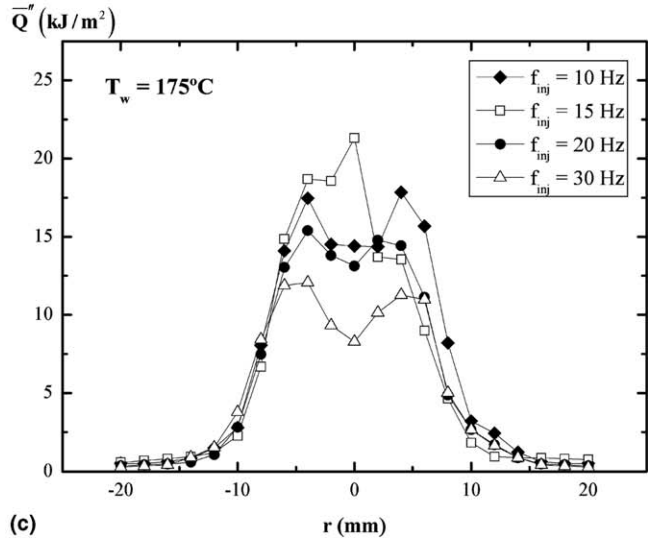

Fig. 12. Radial profiles of the time average wall energy flux.

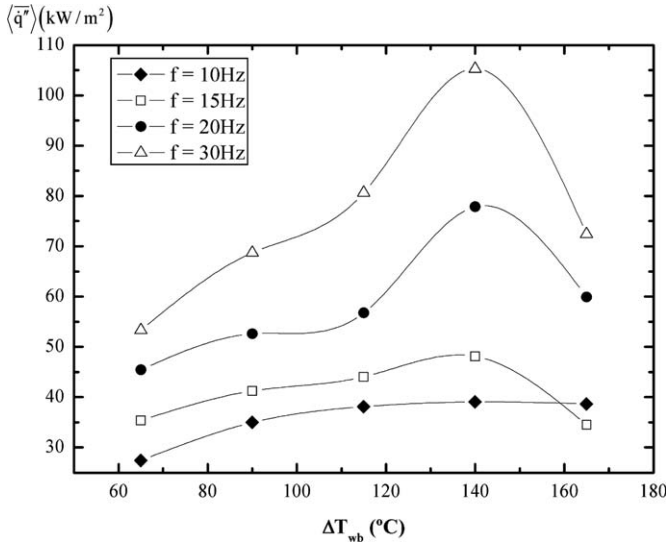

Fig. 13. Overall boiling curves as a function of the injection frequency.

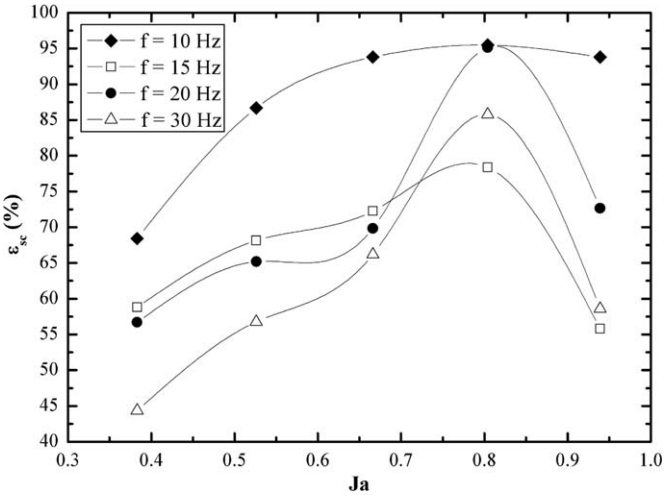

Fig. 14. Variation of the overall cooling efficiency associated with the Jacod number for all frequencies of injection.

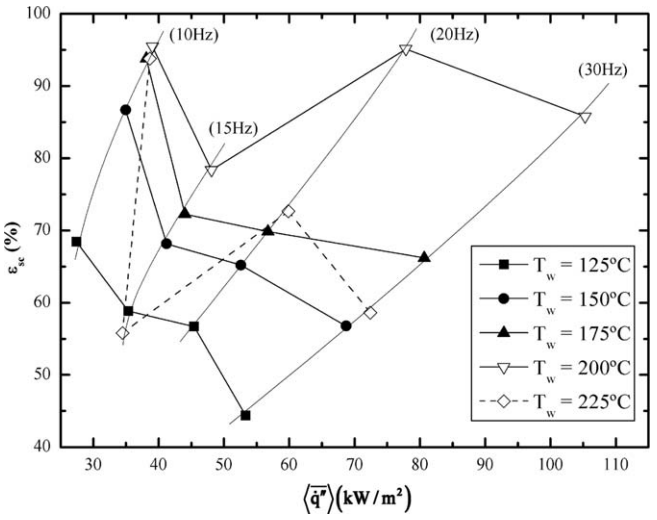

Fig. 15. Spray cooling efficiency versus heat flux for constant surface temperatures.

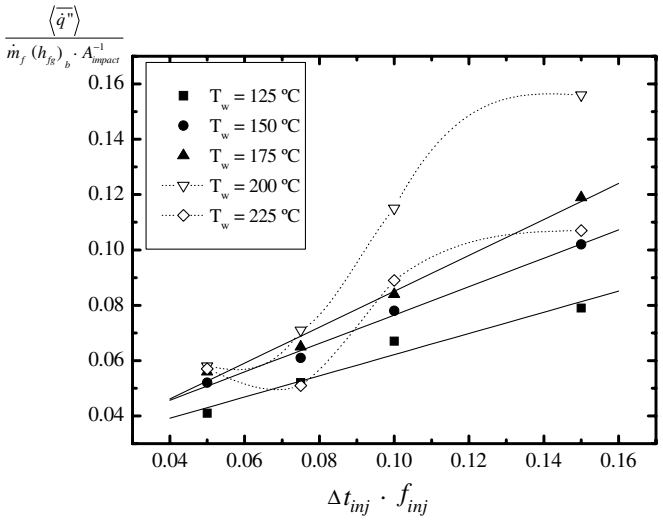

Fig. 16. Total average heat flux as function of the injection frequency for different initial surface temperatures.

Table 4
Coefficients for the total average heat flux linear dependency on the injection frequency

T_w (°C)	a_f	b_f	R^2
125	0.38286	0.02386	0.98
150	0.51314	0.02514	0.996
175	0.64914	0.02014	0.994

$$\frac{\langle\overline{\dot{q}''}\rangle}{\dot{m}_f(h_{fg})_b\cdot A_{impact}^{-1}} = 0.17\cdot\frac{T_w}{T_f}\cdot(\Delta t_{inj}\cdot f_{inj}) - 0.284(\Delta t_{inj}\cdot f_{inj}) + 0.046\cdot\frac{T_w}{T_f}\left(1-0.112\frac{T_w}{T_f}\right) - 0.077 \quad (26)$$

valid for 125 °C $\leqslant T_w \leqslant$ 175 °C and 10 Hz $\leqslant f_{inj} \leqslant$ 30 Hz.

One important result behind relation (26) is the cross correlation coefficient, which accounts for the combined non-linear effects of surface temperature and pulse frequency to enhance the average local cooling effect.

Eq. (26) holds true for the nucleate boiling regime and does not apply to the *overall critical heat flux*. Fig. 17 shows the variation of the overall critical heat flux with the flow rate of liquid supplied to the surface, compared with the results provided by correlations found in the literature for continuous sprays, e.g., [35,38,39] making use of droplet characteristics at impact reported in [24]. The results are normalized by the maximum critical heat flux predicted by each correlation for the mass flow rate of our injector operated at 30 Hz.

The figure shows that the critical heat fluxes obtained with the present multiple-intermittent spray vary linearly with the average mass flow rate of liquid delivered by the nozzle, as in continuous sprays. From this point of view, intermittent injection of the liquid allows better control of the heat removed from the surface without deterioration

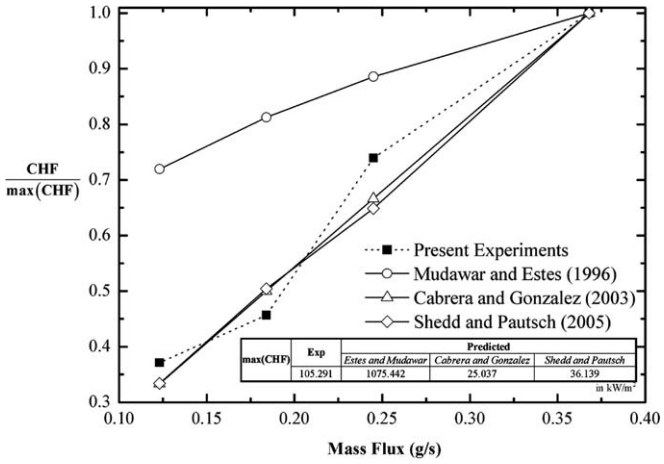

Fig. 17. Overall critical heat flux as a function of the injection frequency.

of the atomization, mainly in practical applications with a wide dynamic range of the heat flux, such as electronic devices. However, an interesting feature is that the slope of the experimental values is similar to that found, either by Cabrera and Gonzalez [38] for water sprays and by Shedd and Pautsch [37] for a spray of FC-72. The correlation provided by Mudawar and Estes [39] shows a much smaller rate of increase, which may be due to the greatly reduced evaporation efficiency of the very dense sprays used by the authors.

Furthermore, Fig. 18 compares the cooling efficiency of the present pulsed spray with estimations from the results reported by Cabrera and Gonzalez [38] and by Shedd and Pautsch [37]. The important conclusion here is that the main benefits of delivering the liquid intermittently is to increase the cooling efficiency, which is attributed to the improved rate of liquid vaporization.

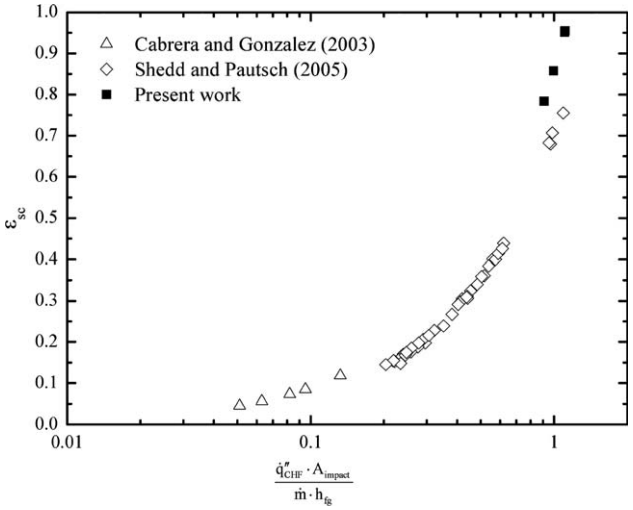

Fig. 18. Comparison of the present experiments with other authors.

4. Summary and conclusions

Intermittent sprays with short pulse duration allows the vapour to be removed more efficiently from the surface, depending on the frequency and duration of injection, and therefore allows attaining larger heat dissipation rates with larger efficiencies. The present work is aimed at providing further insight into the effects of the frequency of injection, which can be used in the development of advanced heat transfer techniques exploring, at the same time, the potential advantages of a hollow cone spray pattern for cooling applications.

The flow configuration is that of a spray of gasoline impacting perpendicularly onto an aluminium flat plate located at 55 mm. The transient behaviour of atomized droplets which is induced by pressure variations induced by pintle-opening has been characterized based on time resolved measurements of droplet size, velocity and number density downstream the nozzle. The frequency of injection mainly affects locations far from the geometrical axis of the spray, where droplets have smaller velocities and, therefore, are more sensitive to drag forces with the air flow induced by the presence of the wall. The resulting effect is the formation of a central region where the heat transfer is influenced by the interaction of impacting droplets with a dynamic liquid film and an outer region where impact conditions are highly transient and single-phase heat transfer is dominant.

Analysis is based on detailed spatial resolved measurements of the instantaneous surface temperature during the period of injection. The experiments were conducted at prescribed temperatures at the start of injection ranging from 125 °C to 225 °C, which cover the nucleate/boiling ($T_b < T_w < T_{Nukiyama}$) and the transition ($T_{Nukiyama} < T_w < T_{Leidenfrost}$) regimes of heat transfer. The frequency of injection is varied from 10 Hz to 30 Hz with durations of 5 ms, corresponding to duty cycles up to 15%.

Local maxima of instantaneous temperature and heat flux increase when the frequency of injection increases from 10 Hz to 20 Hz, but decreases with a further increase of frequency, as a clear indication of the interaction between successive intermittent injections. Integration of time average heat flux over the entire area of impact allows remove from the analysis the complex interactions between neighbouring droplets which depend on injection conditions. Results show the total heat flux follows the behaviour of typical boiling curves with an *Overall Nukiyama Temperature* at the transition from an *overall* heat transfer regime dominated by nucleate boiling to an intermittent transition regime.

The heat transfer in the nucleate boiling regime is shown to be dominated by a thin film boiling mechanism which leads to breakdown of the liquid at a nearly constant surface temperature, regardless of frequency or any other spray conditions. While at low frequencies this regime is not limited neither by the delivery of liquid to the surface, nor by the removal of vapour from the surface, at higher frequencies it is triggered by enhanced vaporization induced by piercing and mixing the liquid film. The experiments allow estimating a correlation for the overall average heat flux removed from the surface within the nucleate regime:

$$\frac{\langle \dot{\overline{q''}} \rangle}{\dot{m}_f (h_{fg})_b \cdot A_{impact}^{-1}} = 0.17 \cdot \frac{T_w}{T_f} \cdot (\Delta t_{inj} \cdot f_{inj}) - 0.284(\Delta t_{inj} \cdot f_{inj}) + 0.046 \cdot \frac{T_w}{T_f}\left(1 - 0.112\frac{T_w}{T_f}\right) - 0.077$$

which accounts for the combined non-linear effects of surface temperature and pulse frequency. The critical heat flux is shown to be well predicted by correlations reported in the literature for continuous low-density sprays of water and dielectric liquids. However, it is shown that the main benefit of delivering the liquid intermittently is to increase the cooling efficiency, which is attributed to the improved rate of liquid vaporization.

Acknowledgements

The authors acknowledge the financial contribution of the National Foundation of Science and Technology at the Ministry for Science and Technology through project POCTI/EME/57944/2004. The author M. R. O. Panão is also provided with financial support through PhD grant SFRH/BD/18669/2004.

Appendix A. Lateral heat conduction effects

To evaluate the lateral heat conduction effects, the heat conduction energy equation is written in cylindrical coordinates as:

$$\rho_w C_{p_w} \frac{\partial T_w}{\partial t} = k_w \left(\frac{\partial^2 T_w}{\partial r^2} + \frac{1}{r}\frac{\partial T_w}{\partial r} + \frac{1}{r^2}\frac{\partial^2 T_w}{\partial \phi^2} + \frac{\partial^2 T_w}{\partial z^2} \right) \quad \text{(A1)}$$

where ρ_w, C_{pw} and k_w are the wall density, specific heat and thermal conductivity, T_w is the wall top surface temperature, and finally r, ϕ and z are the top surface plane and normal (from top) coordinates, respectively (Fig. A1).

Taking $\theta(r,\phi,z,t) = T_w(r,\phi,z,t) - T_w(r,\phi,z,0)$ and assuming axisymmetry, variations with ϕ are eliminated and Eq. (A1) writes:

$$\underbrace{\rho_w C_{p_w} \frac{\partial \theta}{\partial t}}_{\text{total heat exchanged}} = k_w \left(\underbrace{\frac{\partial^2 \theta}{\partial r^2} + \frac{1}{r}\frac{\partial \theta}{\partial r}}_{\text{lateral heat conduction}} + \underbrace{\frac{\partial^2 \theta}{\partial z^2}}_{\text{normal heat conduction}} \right) \quad \text{(A2)}$$

Fig. A1a depicts the eroding type fast response thermocouple made of 2 ribbons of chromel and alumel,

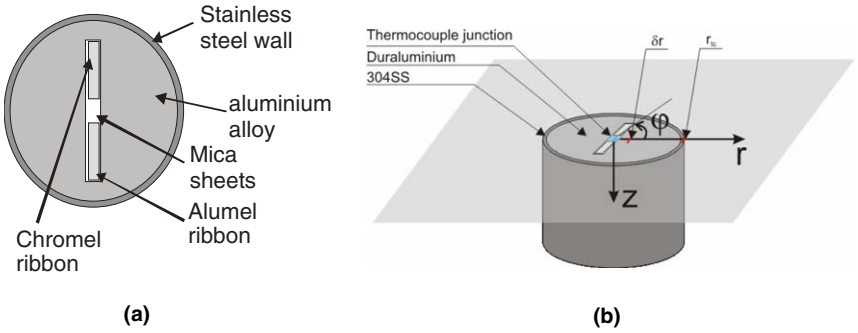

Fig. A1. (a) Configuration of the eroding type thermocouple (b) embedded into an aluminium surface.

insulated by mica sheet, surrounded by the same material of the wall where it is embedded and, finally, packed in a 304SS alloy ultra-thin tube. Fig. A1b represents the heat flux directions and two characteristic points that will be used in the analysis: δr for small perturbations near the thermocouple junction (Section A.1) due to lateral heat conduction effects; and r_{tc} to account for the overall thermal resistance (R_t) due to the presence of different materials (Section A.2).

A.1. Lateral heat conduction near the thermocouple junction

To quantify the influence of lateral heat fluxes in the vicinity of the thermocouple junction, the total heat exchange and lateral heat conduction terms of Eq. (A2) are integrated over a distance δr equal to 10% of the thermocouple radius:

$$\dot{q}_t''^{r} = \rho_w C_{p_w} \int_0^{\delta r} \frac{\partial T_w}{\partial t}\,dr \tag{A3}$$

$$\dot{q}_l''^{r} = k_w \int_0^{\delta r} \left[\frac{\partial^2\theta}{\partial r^2} + \frac{1}{r}\frac{\partial\theta}{\partial r}\right] dy \tag{A4}$$

Since the instantaneous surface temperature at any point in the substrate is given by

$$\theta(r,z,t) = \int_0^t \frac{\partial\theta}{\partial t^*}\,dt^* \tag{A5}$$

Substituting Eq. (A5) in (A4), the lateral heat conduction per unit area becomes

$$\dot{q}_l''^{r} = \alpha_w \left[\int_0^t \frac{\partial^3}{\partial r^3}\rho_w C_{p_w}\int_0^{\delta r}\frac{\partial\theta}{\partial t^*}\,dr\,dt^* + \int_0^t \frac{\partial}{\partial r}\left(\frac{1}{r}\frac{\partial}{\partial r}\right)\rho_w C_{p_w}\int_0^{\delta r}\frac{\partial\theta}{\partial t^*}\,dr\,dt^*\right] \tag{A6}$$

which, with the aid of Eq. (A3), reduces to

$$\dot{q}_l''^{r} = \alpha_w \left[\int_0^t \frac{\partial^3 \dot{q}_t''^{r}}{\partial r^3}\,dt^* + \int_0^t \frac{\partial}{\partial r}\left(\frac{1}{r}\frac{\partial \dot{q}_t''^{r}}{\partial r}\right) dt^*\right] \tag{A7}$$

The following step considers that the ratio between the total heat flux integrated in δr and the normal heat flux obtained by a one-dimensional analysis can be reasonably described by a parabolic function as

$$\frac{\dot{q}_t''^{y}}{\dot{q}_{1D}''} = A + By + Cy^2 \tag{A8}$$

Therefore, if the lateral heat conduction is only a small fraction of the total heat flux removed by the spray at impact, its value would be given by the 1D analysis in Section 2.2. Following Buttsworth and Jones [40], Eqs. (A7) and (A8) can be used to obtain a better estimate as

$$\dot{q}_l''^{r} = \alpha_w[B + 2C(\delta r + 1)] \cdot \int_0^t \dot{q}_{1D}''^{0}(t^*)\,dt^* \tag{A9}$$

where $\dot{q}_{1D}''^{0}$ is the instantaneous heat flux calculated by the Reichelt et al. method [27]. Thus, a more accurate relation for the total convective heat flux at the thermocouple junction is given by

$$\dot{q}_{1D}''^{i}(t) = \dot{q}_{1D}''^{0}(t) - \alpha_w[B + 2C(\delta r + 1)]\int_0^t \dot{q}_{1D}''^{0}(t^*)\,dt^* \tag{A10}$$

Fig. A2 depicts the magnitude of the values obtained for B and C, while Fig. A3 shows the histogram of the residual sum of squares (RSS) between $\dot{q}_{1D}''^{0}(t)$ and $\dot{q}_{1D}''^{i}(t)$ as

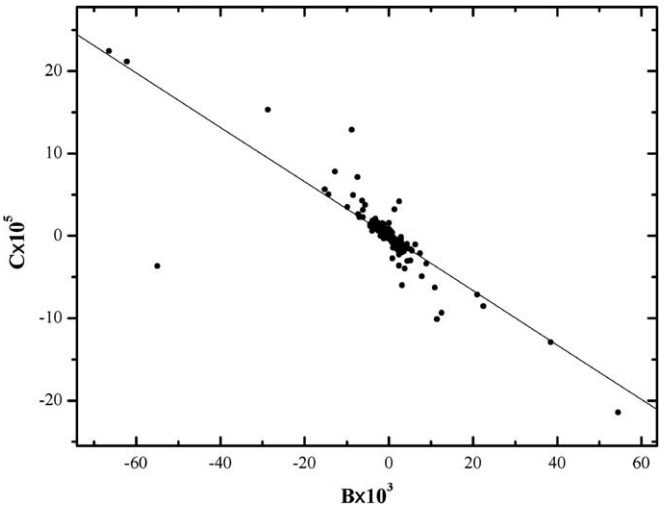

Fig. A2. Magnitude of constants B and C for the parabolic correlation between the total convective heat flux and the heat flux assuming one-dimensional heat conduction.

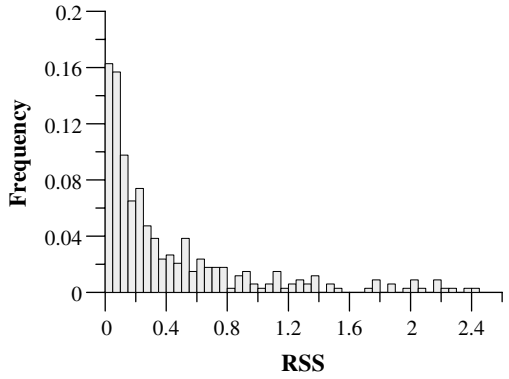

Fig. A3. Residual sum of squares between the 1D instantaneous heat flux and the estimated heat flux accounting for lateral conduction effects.

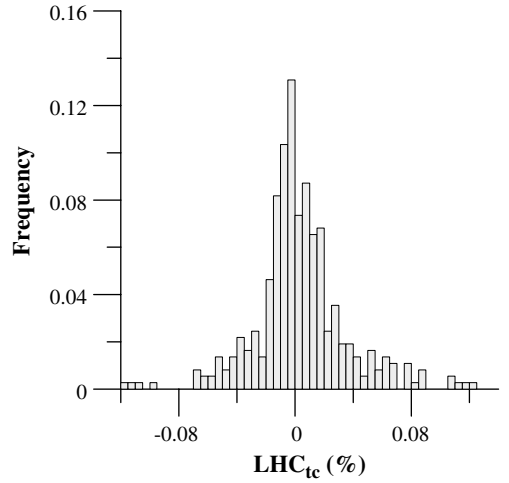

Fig. A4. Ratio (in percentage) between the lateral heat flux at the thermocouple boundary and the 1D instantaneous heat flux.

$$\mathrm{RSS} = \sqrt{\sum_{j=1}^{N} \left(\dot{q}''^{0}_{1\mathrm{D}_j} - \dot{q}''^{i}_{1\mathrm{D}_j} \right)^2} \tag{A11}$$

with median value of 0.223, which means that lateral heat conduction effects are negligible near the thermocouple junction.

A.2. Lateral heat conduction due to overall thermal resistance at thermocouple edge

The aluminium substrate involving the thermal junction is enfolded by a 304SS alloy (see Fig. A1b), for which inaccuracies may also be caused by significant heat flux at the thermocouple boundaries (r_{tc}) due to the overall thermal resistance (R_t). At the boundary of the thermocouple bead, the heat transfer rate $\dot{q}''_{tc}(t)$ between the junction $T_w^{\text{junction}}(t)$ and the boundary $T_w^{y_{tc}}(t)$ can be written as in [41] by

$$\dot{q}''_{tc}(t) = \frac{T_w^{\text{junction}}(t) - T_w^{y_{tc}}(t)}{R_t} \tag{A12}$$

where R_t is the overall thermal resistance

$$R_t = \frac{r_{tc} - \delta r_{304SS}}{k_w} + \frac{\delta r_{304SS}}{k_{304SS}} \tag{A13}$$

where r_{tc} is the radius of the thermocouple (1.5875 mm), δr_{304SS} is the thickness of the stainless steel pack (0.186 mm), k_w and k_{304SS} are the thermal conductivities of the aluminium and stainless steel alloy, 164 W/mK and 13.5 W/mK, respectively. It is noteworthy that the aluminium substrate is made of the same material as the wall.

The temperature variation at r_{tc} is estimated from linear interpolation of measurements at adjacent points and once calculated the lateral heat flux is further compared with the normal 1D instantaneous heat flux calculated by the method of Reichelt et al. [27]:

$$\mathrm{LHC}_{tc} = \frac{\dot{q}''_{tc}}{\dot{q}''^{0}_{1D}} \times 100\% \tag{A14}$$

where LHC_{tc} stands for Lateral Heat Conduction at r_{tc}. The results are depicted in the histogram of Fig. A4.

Fig. A4 shows that the lateral heat conduction effect is negligible compared to the assumed one-dimensional heat conduction.

References

[1] I. Mudawar, Assessment of high-heat-flux thermal management schemes, IEEE Trans. Compon. Pack. Technol. 24 (2) (2001) 122–140.
[2] M.R.O. Panão, A.L.N. Moreira, Experimental study of the flow regimes resulting from the impact of an intermittent gasoline spray, Exp. Fluids 37 (6) (2004) 834–855.
[3] B. Richter, K. Dullenkopf, H.-J. Bauer, Investigation of secondary droplet characteristics produced by an isooctane drop chain impact onto a heated piston surface, Exp. Fluids 39 (2005) 351–363.
[4] C. Tropea, I.V. Roisman, Modeling of spray impact on solid surfaces, Atomization Sprays 10 (2000) 387–408.
[5] G.E. Cossali, M. Marengo, M. Santini, Multiple drop impact on heated surface, Ninth International Conference on Liquid Atomization and Spray Systems, Sorrento, Italy, 2003.
[6] J.D. Bernardin, I. Mudawar, Film boiling heat transfer of droplet streams and sprays, Int. J. Heat Mass Transfer 40 (11) (1997) 2579–2593.
[7] I.V. Roisman, C. Tropea, Fluctuating flow in a liquid layer and secondary spray created by an impacting spray, Int. J. Multiphase Flow 21 (2005) 179–200.
[8] M.R.O. Panão, A.L.N. Moreira, Flow characteristics of spray impingement in PFI injection systems, Exp. Fluids 39 (2005) 364–374.
[9] B. Horacek, K.T. Kiger, J. Kim, Single nozzle spray cooling heat transfer mechanisms, Int. J. Heat Mass Transfer 48 (2005) 1425–1438.
[10] K.A. Estes, I. Mudawar, Comparison of two-phase electronic cooling using free jets and sprays, J. Electron. Pack. 117 (1995) 323–332.
[11] W. Jia, H.-H. Qiu, Experimental investigation of droplet dynamics and heat transfer in spray cooling, Exp. Therm. Fluid Sci. 27 (2003) 829–838.
[12] A.C. Cotler, E.R. Brown, V. Dhir, M.C. Shaw, Chip-level spray cooling of an LD-MOSFET RF power amplifier, IEEE Trans. Compon. Pack. Technol. 27 (2004) 411–416.
[13] M.R. Pais, L.C. Chow, E.T. Mathefdey, Surface roughness and its effects on the heat transfer mechanism in spray cooling, ASME J. Heat Transfer 114 (1992) 211–219.

[14] B.M. Pikkula, J.H. Torres, J.W. Tunnell, B. Anvari, Cryogen spray cooling: effects of droplet size and spray density on heat removal, Lasers Sur. Med. 28 (2001) 103–112.
[15] G. Aguillar, B. Majaron, E. Karapetian, E.J. Lavernia, J.S. Nelson, Experimental study of cryogen spray properties for application in dermatologic laser surgery, IEEE Trans. Biomed. Eng. 50 (7) (2003) 863–869.
[16] B. Kao, K.M. Kelly, G. Aguillar, Y. Hosaka, R.J. Barr, J.S. Nelson, Evaluation of cryogen spray cooling exposure on in vitro model human skin, Lasers Sur. Med. 34 (2004) 146–154.
[17] J.W. Tunnell, J.H. Torres, B. Anvari, Methodology for estimation of time-dependent surface heat flux due to cryogen spray cooling, Ann. Biomed. Eng. 30 (2002) 19–33.
[18] J. Ramirez-San-Juan, A.T. Tuqan, K.M. Kelly, J.S. Nelson, G. Aguillar, Evaluation of sub-zero and residence times after continuous versus multiple intermittent cryogen spray cooling exposure on human skin phantom, in: Proceedings of IMECE04, 2004 ASME International Mechanical Engineering Congress and Exposition, California, USA, November 13–20 2004.
[19] B. Marajon, L.O. Svaasand, G. Aguilar, J.S. Nelson, Intermittent cryogen spray cooling for optimal heat extraction during dermatologic laser treatment, Phys. Med. Biol. 47 (2002) 3275–3288.
[20] A.C. Alkidas, Intake-valve temperature and the factors affecting it, SAE Technical Paper 971729, 1997.
[21] P.J. Shayler, M.J.F. Colechin, A. Scarisbrick, Heat transfer measurements in the intake port of a spark ignition engine, SAE Technical Paper 960273, 1996.
[22] P.J. Shayler, M.J.F. Colechin, A. Scarisbrick, Fuel film evaporation and heat transfer in the intake port of an SI engine, SAE Technical Paper 961120, 1996.
[23] A.L.N. Moreira, J. Carvalho, M.R.O. Panão, The effects of fuel impact on mixture preparation in SI engines with port fuel injection, SAE Technical Paper Series, 2005-24-083.
[24] M.R.O. Panão, A.L.N. Moreira, Thermo- and fluid dynamics characterization of spray cooling with pulsed sprays, Exp. Therm. Fluid Sci. 30 (2005) 79–96.
[25] W. Verkruysse, B. Marajon, G. Aguillar, L. O Svaasand, J.S. Nelson, Dynamics of cryogen deposition relative to heat extraction rate during cryogen spray cooling, Proc. SPIE 3907 (2000) 37–48.
[26] R.W. Tate, Some problems associated with the accurate representation of droplet size distributions, in: Proceedings of the Second International Conference on Liquid Atomization and Spray Systems, Madison, USA, 1982.
[27] L. Reichelt, U. Meingast, U. Renz, Calculating transient wall heat flux from measurements of surface temperature, Int. J. Heat Mass Transfer 45 (2002) 579–584.
[28] X.D. Chen, S.K. Nguang, The theoretical basis of heat flux sensor, J. Appl. Math. Decis. Sci. 7 (2003) 1–10.
[29] V.G. Labeish, Thermohydrodynamic study of a drop impact against a heated surface, Exp. Therm. Fluid Sci. 8 (1994) 181–194.
[30] J.D. Naber, P.V. Farrell, Hydrodynamics of droplet impingement on a heated surface, SAE Technical Papers 930919, 1993.
[31] J.C. Chen, K.K. Hsu, Heat transfer during liquid contact on superheated surfaces, J. Heat Transfer 117 (1995) 693–697.
[32] G. Aguillar, B. Marajon, W. Verkruysse, Y. Zhou, J.S. Nelson, E.J. Lavernis, Theoretical and experimental analysis of droplet diameter, temperature and evaporation rate evolution in cryogen sprays, Int. J. Heat Mass Transfer 44 (2001) 3201–3211.
[33] S.C. Yao, T.L. Cox, A general heat transfer correlation for impacting water sprays on high-temperature surfaces, Exp. Heat Transfer 15 (2002) 207–219.
[34] I. Kopchikov, G. Voronin, T. Kolach, D. Labuntsov, P. Lebedev, Liquid boiling in a thin film, Int. J. Heat Mass Transfer 12 (1969) 791–796.
[35] A.G. Pautsch, T.A. Shedd, Spray impingement cooling with single- and multiple-nozzle arrays. Part I: visualization and empirical models, Int. J. Heat Mass Transfer 48 (2005) 3176–3184.
[36] D. Rini, Ruey-Hung Chen, L.C. Chow, Bubble behavior and nucleate boiling heat transfer in saturated FC-72 spray cooling, J. Heat Transfer 124 (February) (2002) 63–72.
[37] T.A. Shedd, A.G. Pautsch, Spray impingement cooling with single- and multiple-nozzle arrays. Part II: heat transfer data using FC-72, Int. J. Heat Mass Transfer 48 (2005) 3167–3175.
[38] E. Cabrera, J.E. Gonzalez, Heat flux correlation for spray cooling in the nucleate boiling regime, Exp. Heat Transfer 16 (2003) 19–44.
[39] I. Mudawar, K.A. Estes, Optimizing and predicting CHF in spray cooling of a square surface, J. Heat Transfer 118 (1996) 672–679.
[40] D.R. Buttsworth, T.V. Jones, A fast-response high spatial resolution total temperature probe using a pulsed heating technique, J. Turbomach. 120 (1998) 601–607.
[41] A. Bejan, Heat Transfer, Wiley, New York, 1993, pp.32–35.